NAVAL POSTGRADUATE SCHOOL
Monterey, California

THESIS

SIMULATION OF THE COUPLED ATMOSPHERIC AND OCEANIC BOUNDARY LAYER MODEL DURING MILDEX

by

Joseph W. Swaykos

December 1984

Thesis Advisor: R.W. Garwood

Approved for public release; distribution is unlimited

REPORT DOCUMENTATION PAGE		READ INSTRUCTIONS BEFORE COMPLETING FORM
1. REPORT NUMBER	2. GOVT ACCESSION NO.	3. RECIPIENT'S CATALOG NUMBER
4. TITLE (and Subtitle) Simulation of the Coupled Atmospheric and Oceanic Boundary Layer Model During MILDEX		5. TYPE OF REPORT & PERIOD COVERED Master's Thesis December 1984 6. PERFORMING ORG. REPORT NUMBER
7. AUTHOR(s) Joseph W. Swaykos		8. CONTRACT OR GRANT NUMBER(s)
9. PERFORMING ORGANIZATION NAME AND ADDRESS Naval Postgraduate School Monterey, CA 93943		10. PROGRAM ELEMENT, PROJECT, TASK AREA & WORK UNIT NUMBERS
11. CONTROLLING OFFICE NAME AND ADDRESS Naval Postgraduate School Monterey, CA 93943		12. REPORT DATE December 1984 13. NUMBER OF PAGES 67
14. MONITORING AGENCY NAME & ADDRESS(if different from Controlling Office)		15. SECURITY CLASS. (of this report) 15a. DECLASSIFICATION/ DOWNGRADING SCHEDULE

16. DISTRIBUTION STATEMENT (of this Report)

Approved for public release; distribution is unlimited

17. DISTRIBUTION STATEMENT (of the abstract entered in Block 20, if different from Report)

18. SUPPLEMENTARY NOTES

19. KEY WORDS (Continue on reverse side if necessary and identify by block number)

Coupled Boundary Layer Model
Atmospheric Boundary Layer
MILDEX
Air-Sea Interaction
Oceanic Boundary Layer

20. ABSTRACT (Continue on reverse side if necessary and identify by block number)

A coupled, oceanic-atmospheric boundary layer model which provides single-station prediction capability is evaluated relative to boundary layer observations. The model is initialized and verified using data obtained during the 1983 Mixed Layer Dynamics Experiment (MILDEX). Model prediction of inversion height, lifting condensation level, air and sea temperatures, specific humidity and mixed layer depth are

compared with observations. A significant model shortcoming is the over-prediction of cloud thickness. Consequently, shortwave radiation at the ocean surface is too low and the predicted ocean mixed layer depths are not realistic. Oceanic predictions resulting from independent specification of surface radiation more closely resembled observed oceanic variations. Atmospheric boundary layer model reformulation is required to alleviate the cloud thickness/shortwave radiation problem.

Approved for public release; distribution is unlimited.

Simulation of the Coupled Atmospheric and Oceanic Boundary Layer Model During MILDEX

by

Joseph W. Swaykos
Lieutenant Commander, U.S. Navy
B.S., United States Naval Academy, 1976
M.S., University of Southern California, 1982

Submitted in partial fulfillment of the
requirements for the degree of

MASTER OF SCIENCE IN METEOROLOGY AND OCEANOGRAPHY

from the

NAVAL POSTGRADUATE SCHOOL
December 1984

ABSTRACT

A coupled, oceanic-atmospheric boundary layer model which provides single-station prediction capability is evaluated relative to boundary layer observations. The model is initialized and verified using data obtained during the 1983 Mixed Layer Dynamics Experiment (MILDEX). Model prediction of inversion height, lifting condensation level, air and sea temperatures, specific humidity and mixed layer depth are compared with observations. A significant model shortcoming is the over-prediction of cloud thickness. Consequently, shortwave radiation at the ocean surface is too low and the predicted ocean mixed layer depths are not realistic. Oceanic predictions resulting from independent specification of surface radiation more closely resembled observed oceanic variations. Atmospheric boundary layer model reformulation is required to alleviate the cloud thickness/shortwave radiation problem.

ACKNOWLEDGEMENTS

I wish to thank Dr. R.W. Garwood, Department of Oceanography and Dr. K.L. Davidson, Department of Meteorology for their guidance, encouragement and time throughout this study. Special appreciation is extended to Patricia A. Boyle for her assistance in developing the the variables used in model initialization. Additionally, Mr. T. Stanton was extremely helpful in obtaining and interpreting oceanic data which was graciously provided by Scripps Institute of Oceanography.

Above all, I would like to express my sincerest gratitude to my wife Linda and to my children, Joseph and Catherine. This work would have been impossible without their patience, understanding and support.

TABLE OF CONTENTS

LIST OF TABLES

LIST OF FIGURES

I. INTRODUCTION

All aspects of naval operations are affected by the adjacent ocean/atmosphere environment. The performance of weapons systems operating on the principles of electro-optical (EO) and electromagnetic (EM) physics are dependent upon the existing atmospheric conditions in the marine atmospheric boundary layer (MABL). Those systems whose operation is governed by water borne acoustic paths are dependent upon the environmental conditions in the ocean boundary layer. Aside from the exceptionally severe weather phenomena so commonly associated with environmental dynamics, the complex weapons systems in use throughout the fleet are affected by routine environmental conditions and subtle changes therein as well as by the renowned extremes.

Atmospheric dynamics will alter the vertical profiles of temperature, humidity and pressure which are the variables affecting the refractivity of the atmosphere. The vertical gradient of refractivity is the critical factor in the presence of phenomena such as ducting, subrefraction, superrefraction, frequency dependencies and their impact upon the performance of electro-optical and electromagnetic systems.

Oceanic dynamics manifest as vertical variations in temperature, pressure and salinity affect the sound speed profile. As the most critical factor in determining the propagation of acoustic energy, variations in the sound speed profile as a function of depth will result in phenomena such as surface ducting and convergence zones and will determine cutoff frequencies and optimal source/receiver geometries.

Atmospheric and oceanic boundary layer processes are highly interdependent. The ability to predict their interaction is clearly essential to the tactical commander.

The model evaluated consists of a one dimensional atmospheric model (Davidson et al., 1984) and a one dimensional oceanic boundary layer model (Garwood, 1977). The models were coupled (O'Laughlin, 1982) and demonstrated to realistically simulate boundary layer dynamics (Hervey, 1983). The goal of this study is to assess the ability of a coupled ocean-atmosphere boundary layer model to accurately make such predictions by conducting a boundary layer simulation using oceanic and atmospheric data obtained during the 1983 Mixed Layer Dynamics Experiment (MILDEX).

II. BACKGROUND

A. MOTIVATION

The evolution of the NPS coupled atmospheric and oceanic boundary layer model has reached the developmental stage of being used to predict atmospheric and oceanic dynamics using actual data sets for initialization and comparison with model output. Prior efforts along this model development path include an examination of the coupled model's ability to forecast using real data for initialization and comparison of results in order to determine the adequacy of the coupling (O'Laughlin, 1982). This study concluded that the coupled model did indeed yield fairly accurate results; however, the data sets employed (CEWCOM 1976 and CEWCOM 1978) were inadequate. The inadequacy was a result of the frequent transit of the data gathering vessel, RV ACANIA over significant distances through inhomogeneous water masses.

A follow-on study examined the adequacy of the coupled boundary layer model relative to the performance of the uncoupled atmospheric and oceanic models. The results indicated that the benefits of coupling to the MABL were minor; however, the predictive capability of the OBL was greatly enhanced (Hervey, 1983).

Both studies recommended evaluation with data sets where effects of advection and vessel movement are minimized. Such a data set was obtained during the 1983 Mixed Layer Dynamics Experiment (MILDEX) (Geernaert *et al.*, 1984), conducted from October 24 through November 10, 1983. Data were obtained 3 to 5 November, 1983 in the vicinity of 34 N and 126 W by RV ACANIA (Fig. 2.1). Meteorological data

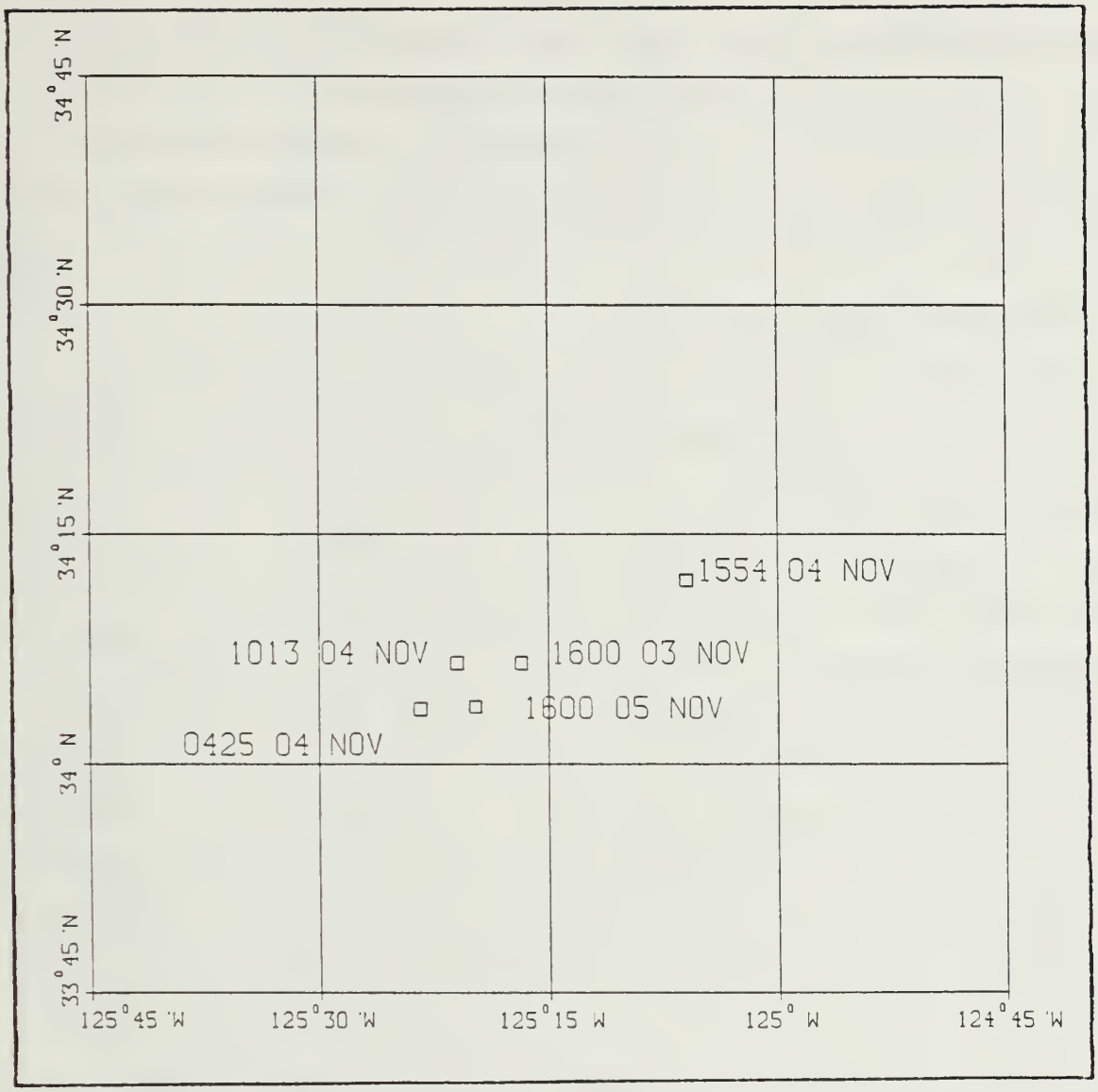

Figure 2.1 Positions of RV ACANIA: 03-05 Nov 1983

consisted of atmospheric pressure, windspeed, temperature, humidity and radiation in the atmospheric surface layer. Profiles of atmospheric wind speed and direction, temperature and humidity using a navaid radiosonde system were also obtained. Additionally, observations of sea state and cloudiness were recorded hourly.

Oceanographic data were obtained with a Neil Brown Instrument System (NBIS) CTD. The device recorded values of temperature, conductivity, depth and dissolved oxygen. Two other research vessels, WACOMA and FLIP acquired data in the vicinity of ACANIA. FLIP was within 2 kilometers of the ACANIA from October 26 through November 9.

B. BOUNDARY LAYER CHARACTERISTICS

The Marine Atmospheric Boundary Layer (MABL) extends from the air-sea interface through a capping inversion typically 100 to 1000m high. The Oceanic Boundary Layer (OBL) extends from the interface to the thermocline, 2 to 50m deep. The MABL is comprised of a cool, moist, turbulent well mixed layer (relative to the upper atmosphere) in which equivalent potential temperature and specific humidity are basically constant with height. At the inversion level a significant change (jump) in the vertical profiles of these variables occurs. The air above the inversion is warmer than that of the mixed layer and is characterized by a lapse rate of increasing temperature as a function of height. Similarly, the air of the free atmosphere is drier than that of the MABL with the moisture content decreasing as a function of height.

The value of the well mixed quantities change over time due to the turbulent fluxes of heat and moisture at the air-sea interface and at the inversion. Turbulent kinetic energy provides the necessary forcing of these processes. The turbulent kinetic energy budget provides the foundation upon which most of the modelling is based. The well mixed nature of the variables in the MABL and OBL imply that heat and moisture are conserved during the mixing process and that the variation with height of the vertical turbulent fluxes of momentum, humidity and heat is linear. Assuming

advection is negligible, these properties permit the modeling of the variation of the variables based solely upon surface and inversion layer height fluxes.

Turbulence at the inversion causes the entrainment of warm, dry air into the MABL and growth of the layer, large (synoptic) scale atmospheric forcing contributes to subsidence. The time rate of change of the height of the MABL is a result of these effects.

An important atmospheric feature is the presence of clouds. If the lifting condensation level (LCL) is lower than the height of the inversion, clouds will be present. A stratus layer in the MABL will vary the amount of solar, shortwave and return long wave radiation in the boundary layer. Such variations will greatly affect the dynamics of the MABL and OBL (Hervey, 1983).

The Oceanic Boundary Layer (OBL) is a turbulent region of the upper ocean bounded by a dynamically stable water mass at its base and by the air-sea interface above. The layer is characterized by constant velocity and density profiles arising from the high degree of turbulence within the layer and a relatively slight amount of turbulence in the underlying stable watermass. Momentum and buoyancy fluxes through the surface provide the energy which results in the boundary layer turbulence.

Density is a function of temperature and salinity, both of which are assumed to be homogeneous in the boundary layer. Since the model will forecast for relatively short periods of time (less than 72 hours), the effects of salinity are assumed to be negligible (Miller, 1976). As in the case of the MABL, the vertical homogeneity of the OBL allows for the modelling of dynamic processes through the use of only the surface and entrainment fluxes. The turbulent kinetic energy budget again serves as the foundation for modeling.

C. MIXED ATMOSPHERIC BOUNDARY LAYER MODEL (MABL)

The atmospheric variables required as input are short-wave radiation, which depends on Julian date, time of day and latitude, inversion height, mixed layer and jump values for equivalent potential temperature and specific humidity. Also the above layer lapse rates for specific humidity and potential temperature, subsidence rate, wind speed and direction within the mixed layer and sea surface temperature are required. In the uncoupled model sea surface temperature is constant. However, the coupled model uses the variations in sea surface temperature as predicted by the OBL model as an input.

Three methods are available for the computation of subsidence (large scale vertical velocity). The methods are the kinematic, the adiabatic and the integration of the moisture budget equation (Q method). The Q method is the most accurate approach given single station data, according to Gleason (1982). It was used for subsidence calculation for this study.

The MABL predicts the evolution of the LCL, inversion height, mixed layer values of equivalent potential temperature and specific humidity, their respective jump values, entrainment rate, short and long wave radiation, friction velocity (U*), and the scaling parameters for temperature and humidity (T* and Q*) for a prescribed period. The model uses a 30 minute time step. The computational steps are depicted in Fig. 2.2.

The time evolution of the conservative variables are predicted using integrated (with respect to height) rate equations (Tennekes and Dreidonks, 1981). These equations are:

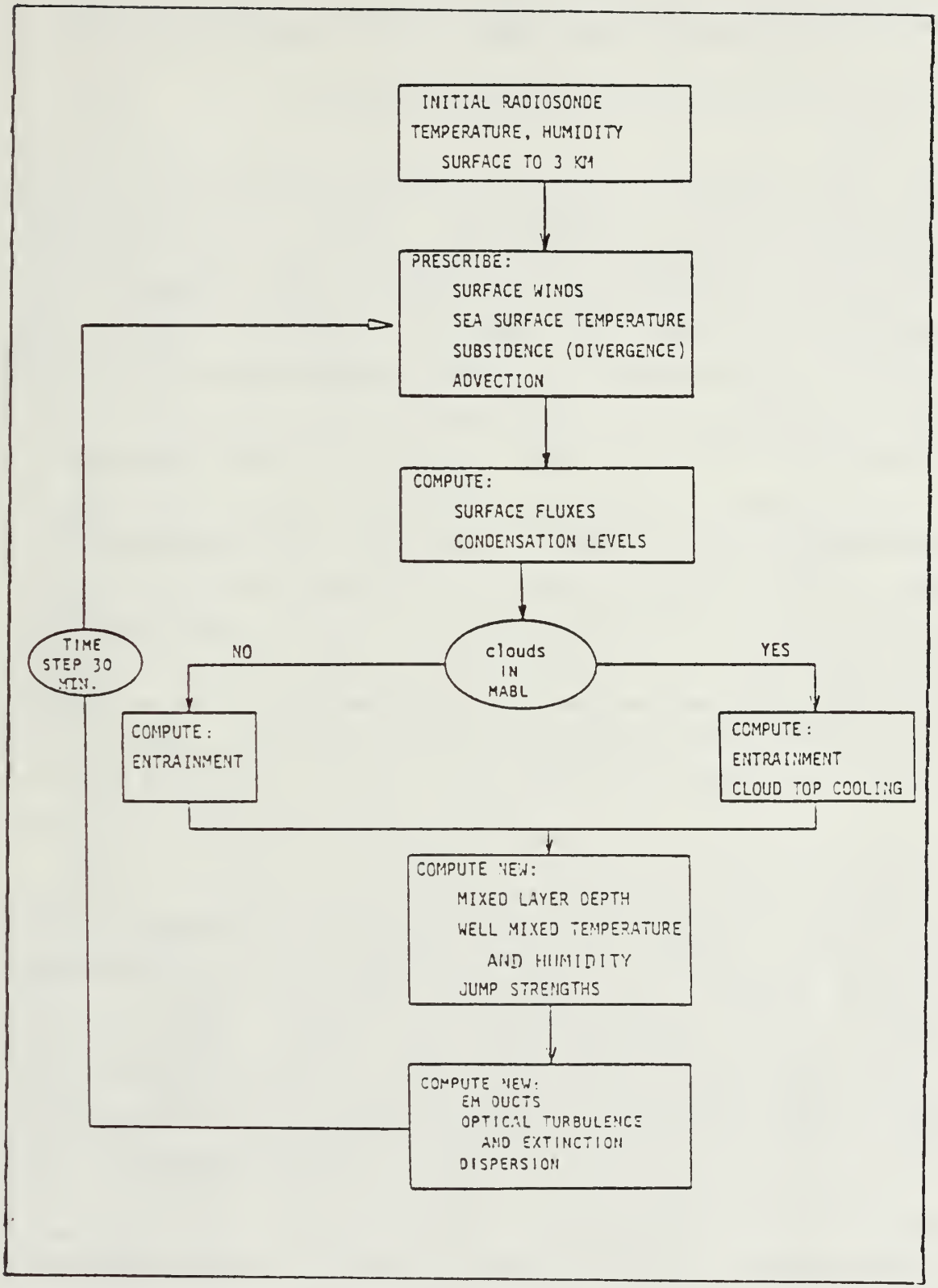

Figure 2.2 MABL Schematic

$$h(Dx/Dt) = (w'x')_o - (w'x')_h + \text{source} \qquad (2.1)$$

$$h(D\Delta x/Dt) = h\Gamma_x(\partial h/\partial t) - (w'x')_o + (w'x')_h - \text{source} \qquad (2.2)$$

where the subscripts zero and h refer to surface and inversion height values, respectively. Gamma (Γ) is the lapse rate above the inversion height and the source term is equal to $-(F_{nh} - F_{no})/\rho C_p$ for $X = \theta$ and equal to zero for $X = q$. The subscripts h and zero refer to inversion height and surface, respectively, Fn is the net radiative flux. The quantity $(\partial h/\partial t)$ is the difference between the time rate of change of the inversion height (dh/dt) and subsidence rate.

The system of equations is closed through the use of Stage and Businger's (1981) entrainment rate parameterization. This is also used in the determination of the temporal evolution of the inversion height. To obtain the entrainment rate, Stage and Businger made a closure assumption that the dissipation rate of turbulent kinetic energy is a fraction (1-A) of the production rate, P:

$$D = (1-A)P \qquad (2.3)$$

The quantity 'A' in essence is the critical flux Richardson number (Ri_{cr}) which separates turbulent from nonturbulent boundary layers. It has been determined through the modeling of dry convective layers that A=0.2. This value is in close agreement to that calculated by Businger (1973) and lies in the middle of the range of critical flux Richardson numbers, 0.15 to 0.25, which were determined by Arya (1972).

Earlier modeling efforts indicated that only 1 to 4 percent of the TKE produced in the boundary layer was used for entrainment. The 0.2 factor however indicates that 20 percent of the TKE is thus utilized.

Bulk aerodynamic formulas are used in the determination of the surface fluxes of momentum, heat, and moisture:

$$U^* = C_d^{1/2} U \tag{2.4}$$

$$T^* = C_\theta^{1/2} (\theta - \theta_0) \tag{2.5}$$

$$q^* = C_e^{1/2} (q - q_0) \tag{2.6}$$

The fluxes are represented by:

$$(\overline{u'w'}) = U^{*2} \tag{2.7}$$

$$(\overline{-T'w'}) = U^* T^* \tag{2.8}$$

$$(\overline{-q'w'}) = U^* q^* \tag{2.9}$$

C_d and C_θ are the stability dependent drag and exchange coefficients. The zero subscript refers to surface values, overbars represent average quantities and primes (') represent fluctuations from mean values.

Long and shortwave radiation fluxes are calculated independently. Modeling of these quantities is extremely difficult. Effects of absorbing aerosols and gases, and of the distribution of cloud droplet size, are nearly impossible to predict. Long wave radiation modeling is based upon empirical relations between the average cloud liquid water content and cloud emissivity. Cloud top net long wave radiative flux L is determined from the Stefan-Boltzman law and cloud top temperature:

$$L_{nh} = \epsilon_c \sigma (T_h^4 - T_{sky}^4) \tag{2.10}$$

The parameter σ is Stefan's constant and the parameter ϵ_c is determined by:

$$\epsilon_c = 1 - \exp(-aW) \qquad (2.11)$$

where ϵ_c is the cloud emissivity, W is the cloud liquid water content, and 'a' is a constant equal to .158 $m^2 g^{-1}$ (Slingo, et al., 1982). Cloud base long wave radiative flux is represented by:

$$L_{nc} = \epsilon_c (Ts^4 - Tc^4) \qquad (2.12)$$

where Ts is the sea surface temperature and Tc is the cloud base temperature. Radiative flux divergence in the air between the sea surface and cloud base is neglected so that $L_{nc} = L_{ns}$. Therefore, the net long wave flux at the surface is given by:

$$F(long) = \sigma(Ts^4 - \epsilon_c \bar{T}^4 - (1-\epsilon_c) T_{sky}^4) \qquad (2.13)$$

where $\bar{T}$ is the average cloud temperature.

For the cloud free condition, the net long wave flux is calculated at z=h and z=0 by integrating the flux emissivity profile as developed by Fleagle and Businger (1980). Quite simply, the net long wave radiative flux is given by:

$$F(long) = Fu - Fd \qquad (2.14)$$

where Fu and Fd represent the net upward and downward radiative fluxes, respectively.

Short wave radiative flux is calculated using the delta-Eddington method described by Joseph et al., (1976).

The solar flux is evaluated over 15 equally spaced (.1um) bands ranging from 0.2 to 1.7 um wavelength. Solar zenith angle as determined from previously described input variables is an essential part of these calculations. Several considerations are essential in modeling shortwave radiative flux. Shortwave extinction is primarily a result of scattering (instead of absorption). Scattering which creates a diffuse source of radiation is due to atmospheric particles, water droplets (in the case of clouds) and sea aerosols. The MABL incorporates the direct and diffuse sources of shortwave radiation in determining the total surface flux. Sea surface reflection of incident shortwave radiation is assigned a value of 10 percent.

Due to the one dimensionality of the model and several assumptions incorporated in the Q method of subsidence determination, atmospheric advection was assigned a value of zero.

D. OCEANIC BOUNDARY LAYER MODEL (OBL)

The OBL model was developed by Garwood (1977). It is a one dimensional, second order bulk model. The model employs the Navier-Stokes equation of motion with the geostrophic component eliminated, the continuity equation (assuming incompressible water), the heat equation derived from the first law of thermodynamics, a nonlinear equation of state and the conservation of salt equation.

The dynamics of the entrainment process determine the rate of deepening or shallowing (retreat) of the mixed layer. The fundamental assumption is that the turbulence of the mixed layer provides the energy required to destabilize and erode the underlying stable water mass (Garwood, 1977). As a result, the turbulent kinetic energy budget provides

the basis for the determination of the entrainment rate. The system of equations is closed via the mean turbulent field modeling of the vertically integrated equations for the individual turbulent kinetic energy components along with the bulk buoyancy and momentum equations.

The OBL model differs from earlier efforts in the following ways. First, the amount of wind generated turbulent kinetic energy to be used in mixing is a function of the ratio of the mixed layer depth to the Obukhov mixing length. Also, viscous dissipation is dependent on a local Rossby number and seperate vertical and horizontal equations for turbulent kinetic energy are used (Garwood, 1977).

Buoyancy conservation employed in the OBL is a generalization of the concepts of heat and salt conservation. The buoyancy equation is a combination of a linearized equation of state, conservation of heat and conservation of salinity equations. Buoyancy is simply defined by:

$$\tilde{b} = (\rho_0 - \tilde{\rho})\, g/\rho_0 \qquad (2.15)$$

where $\tilde{\rho}$ is given by:

$$\tilde{\rho} = \rho_0 \{1 - \alpha(\tilde{\theta} - \theta_0) + \beta(\tilde{S} - S_0)\} \qquad (2.16)$$

and where $\tilde{\theta}, \tilde{S}$, and $\tilde{\rho}$ are instantaneous values of temperature, salinity and density, α and β are expansion coefficients for heat and salt respectively. The zero subscript denotes a constant, representative value.

Parameters required for OBL model initialization include shortwave radiation absorbed from the ocean surface to a depth of one meter, the radiation extinction coefficient for determining the downward heat flux and the critical

Richardson number for a stability adjustment at the base of the mixed layer. Surface boundary conditions require specification of wind speed and direction data, cloud cover, sea surface temperature, dry bulb and dew point temperatures, incident solar radiation and precipitation (P) and evaporation (E) rates.

Bulk aerodynamic formulae are used to calculate the turbulent fluxes of latent heat (Qe) and sensible heat (Qh). Shortwave radiation is calculated as previously described (delta Eddington method). An empirical equation (Husby and Seckel, 1978) is used in the determination of the net back radiation, Qb. The upward heat flux is simply the sum of these fluxes:

$$Qu=Qe+Qh+Qb \qquad (2.17)$$

The net radiation is not simply the difference between the downward and upward fluxes since only a fraction of the incident radiation penetrates the mixed layer. The depth of penetration is a function of turbidity, that is, in coastal regions more energy will be absorbed than in the less turbid, open ocean regions. The fraction of shortwave radiation which is absorbed is conceptually regarded as a contribution to the upward radiation. Therefore, the net heating at the surface is represented by:

$$Qnet=Qu+Rf(Qs)-Qs \qquad (2.18)$$

where Rf is the fraction of incident radiation absorbed in the first meter.

Given Qnet the surface fluxes of buoyancy and momentum can be calculated. At this point the turbulent fluxes of buoyancy, salinity and temperature can be determined by:

$$b'w' = g\{\alpha(T'w') - \beta(s'w')\} \qquad (2.19)$$

$$s'w' = (P-E)So \qquad (2.20)$$

$$T'w' = -Qnet/\rho Cp \qquad (2.21)$$

where So represents a surface salinity.

Temperature and salinity profiles as well as the wind driven horizontal current profiles are required for OBL model initialization. Temperature is considered to be the dominant factor in density variation when compared to the effects of salinity over relatively short time periods such as those encountered in this study (Miller, 1976). The initializing profiles are used in the determination of mixed layer depth. According to the OBL model, mixed layer depth is defined to be the shallowest depth at which the observed density value σt, is $.02\sigma t$ units greater than the density at the surface.

E. COUPLED BOUNDARY LAYER MODEL

The processes outlined in the preceding sections have been combined to form a coupled boundary layer model. The coupling is achieved by matching the atmospheric and oceanic fluxes of momentum, sensible and latent heat and radiation at the air-sea interface, O'Laughlin (1982).

The only oceanic variable which forces the atmospheric model is sea surface temperature. Feedback occurs between several atmospheric variables and sea surface temperature. These include wind stress and the fluxes outlined previously. Conversely, nearly all of the atmospheric variables influence the evolution of the oceanic variables.

1. Model Initialization

Coupled model initialization requires the Julian date, local time of day and latitude. Required atmospheric variables are surface pressure, inversion height, LCL, and mixed layer values of specific humidity and potential temperature. Also required are the inversion "jump" values and above layer lapse rates of potential temperature and specific humidity, vertical velocity (subsidence), and values for temperature and moisture advection. The 10 meter wind direction is also specified. The atmospheric model simply requires wind speed; however, the wind stress calculations needed for the OBL require the direction from which the wind is blowing. These computations lead to the determination of ocean turbulent velocity flux U^{*2} where:

$$\tau_s = \rho_a U^{*2} = \rho_w U_w^{*2} \qquad (2.22)$$

Oceanic variables required for initialization are mixed layer depth, sea surface temperature, temperature jump value at the thermocline and the below layer thermal gradient.

Since atmospheric processes occur on a shorter time scale than oceanic processes, the MABL model is designed with a 30 minute time step whereas the OBL model uses a 60 minute time step. It is assumed that sea surface temperature will not change significantly over a 60 minute period. As a result, the ocean model is incorporated as a subroutine of the atmospheric model and is called every other time step. A schematic of the coupled model is depicted by Fig. 2.3.

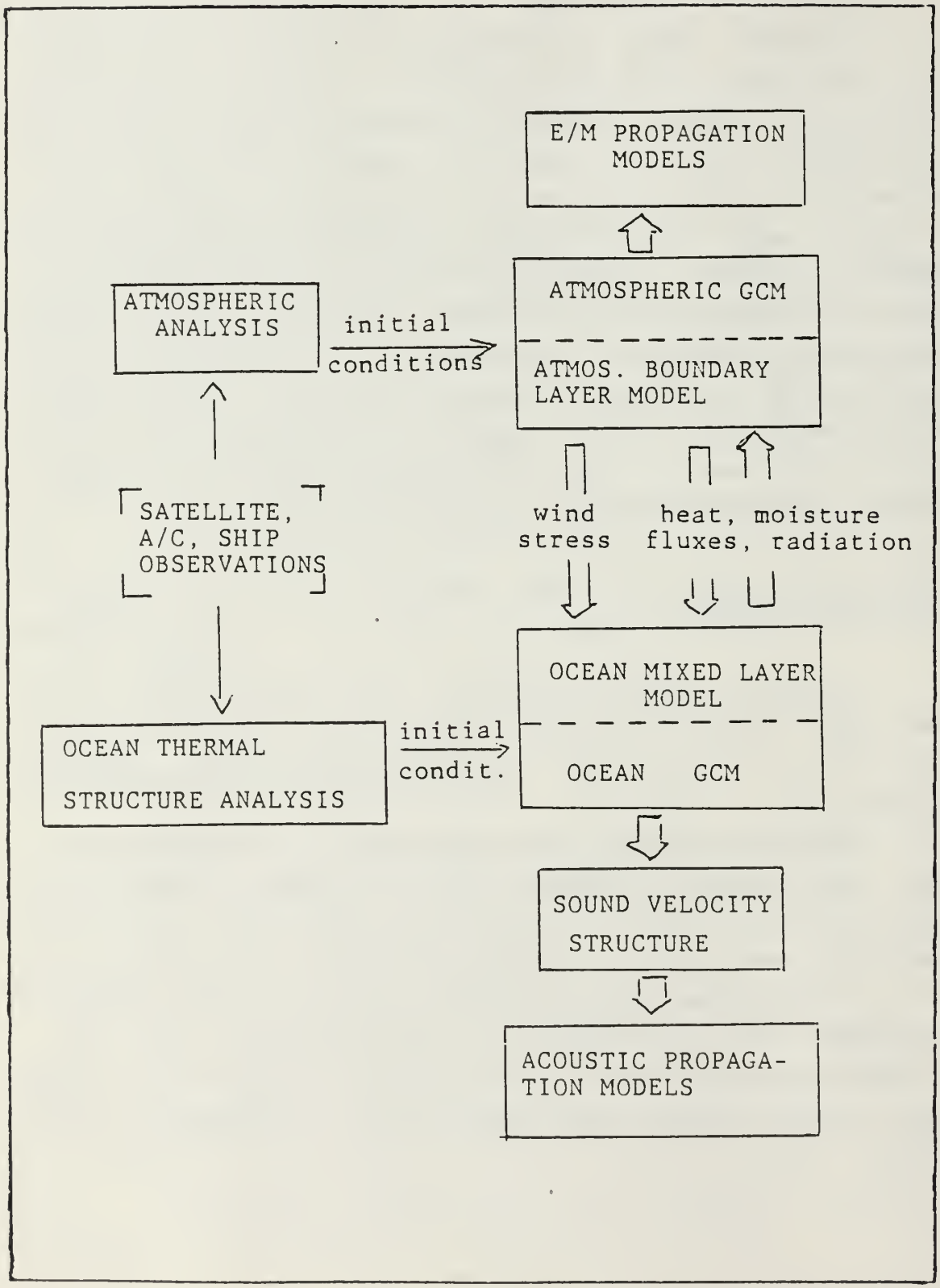

Figure 2.3 Coupled Model Schematic

III. OBSERVATIONS AND RESULTS

A. APPROACH

The data used in this study are from the Mixed Layer Dynamics Experiment (MILDEX), conducted in the Eastern Pacific from 24 October to 10 November 1983. Several criteria were used in selecting the periods for which a sensitivity analysis could be conducted. These included an absence of atmospheric fronts and the availability of frequent and accurate radiosonde and CTD data. Frontal effects; such as, moisture and heat advection are not included in the coupled or uncoupled models. The presence of such activity would therefore impair comparison of the one-dimensional model computations with observed changes in the ocean and the atmosphere in particular.

The necessity of frequent radiosonde and CTD data is critical to the determination of the temporal variation of atmospheric and oceanic variables. The radiosonde data had to be calibrated using measured temperatures at 20 m, which was assumed to be continually within the atmospheric mixed layer. The measured temperatures were converted to potential temperature, assuming a hydrostatic balance. The atmospheric model was then initialized with this potential temperature profile. Several data transmission problems limited the amount of acceptable radiosonde data. Radiosonde launch times coincided with weather satellite overhead time. This time resolution was insufficient to resolve well any synoptic variability in the atmosphere. Oceanic data required no post calibration. However, it too was limited in continuity due to equipment malfunction. As a result, two periods were selected for this analysis.

The first period began at 1600 (Pacific Daylight Time) 03 November and concluded at 1554 04 November. The second period began at 1554 04 November and concluded at 1600 05 November. The data selection process is outlined in Fig. 3.1.

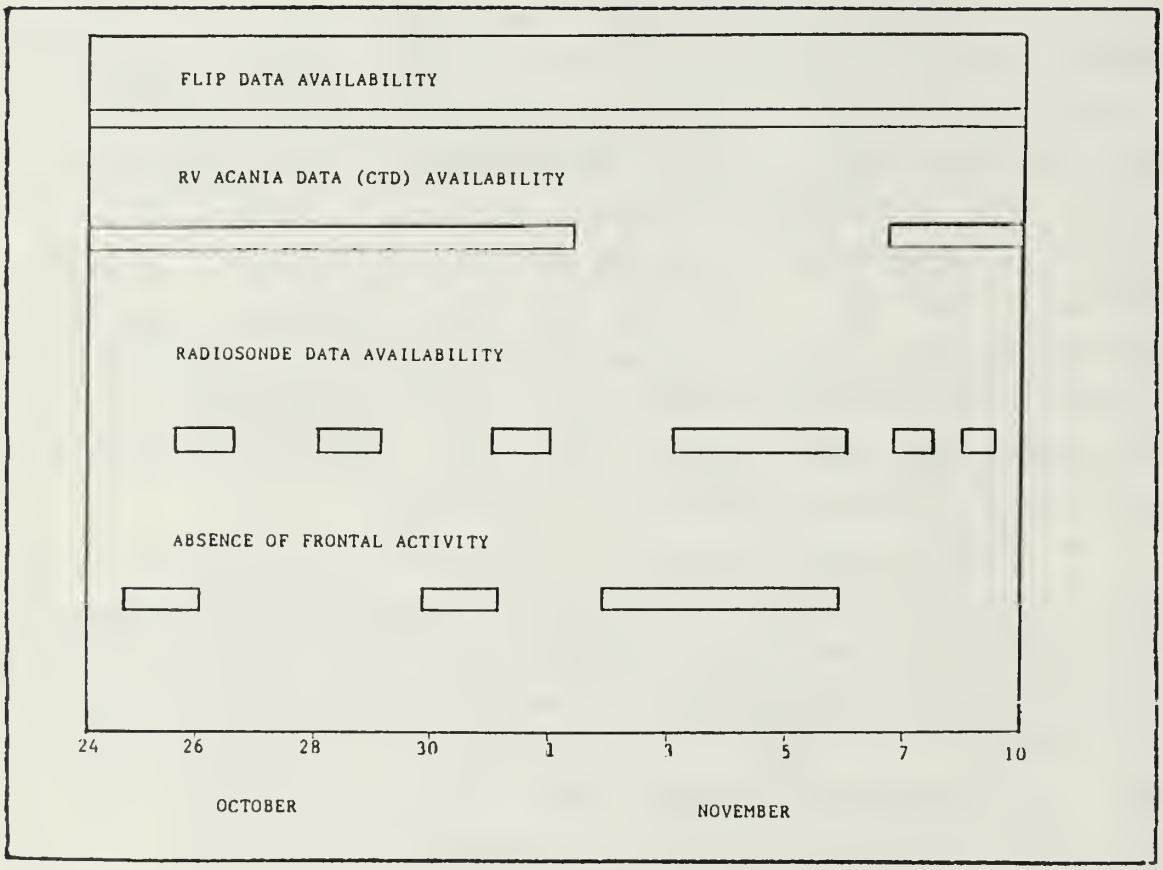

Figure 3.1 Period Selection Criteria

Initial model values for the atmospheric mixed layer, inversion jump and above layer lapse rates for potential temperature and specific humidity were obtained from radiosonde data. Sequential atmospheric soundings were used to determine subsidence rates. Methods for determining subsidence using mean values as well as least squares values are available. Significant differences were not found for the

different approaches; thus, the mean value method was employed in model initialization. Sequential radiosonde profiles preceding and including the profile at the begining of each experimental period were used in subsidence calculations. The remainder of the atmospheric variables required in initialization were tabulated by Geernaert et al., (1984), with the exception of LCL. This value was determined through the use of a Skew T, log P diagram.

Oceanic variables required for initialization were determined from temperature profiles from CTD casts. Mixed layer depth, temperature jump at the thermocline and below layer gradients were thus obtained. The overlapping of oceanic data from ACANIA CTD measurements and FLIP provided a temporally complete data set.

B. CASE I: 1600 PDT 03 NOVEMBER-1554 04 NOVEMBER 1983

1. Uncoupled Model

The values used to initialize Case I are listel in Table I. The uncoupled and coupled model predictions are presented in Figs. 3.2 and 3.3 respectively. In terms of the evolution of the inversion height and LCL, the uncoupled model began with a cloud layer (15 m thickness) with a base at 266 m. Within two hours, the LCL decreased rapidly (from 266 to 126 m) as the inversion height rose. The result was an extremely thick cloud which attained a maximum thickness of 635 m with a base at 183 m, at 0500.

The decrease of the LCL was a result of a combination of factors. The specific humidity increased slightly after initialization followed by a very gradual decrease (.56 g/kg) through 0200. Air temperature decreased 1.9°C from 1600 through 0300. As a result, the air-sea temperature difference increased since the sea surface temperature was held constant. The increase in air-sea temperature

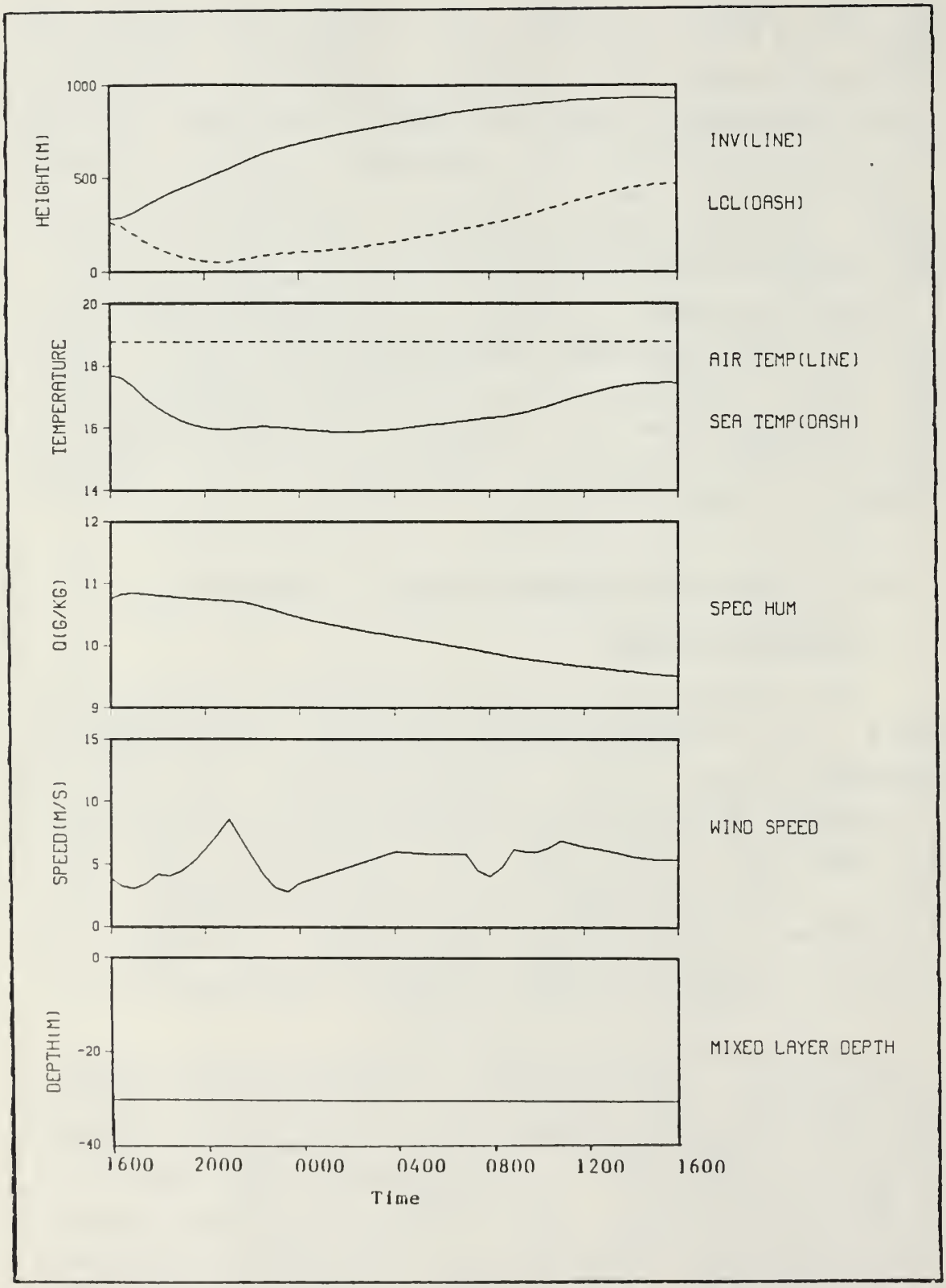

Figure 3.2 Uncoupled Model-Case I

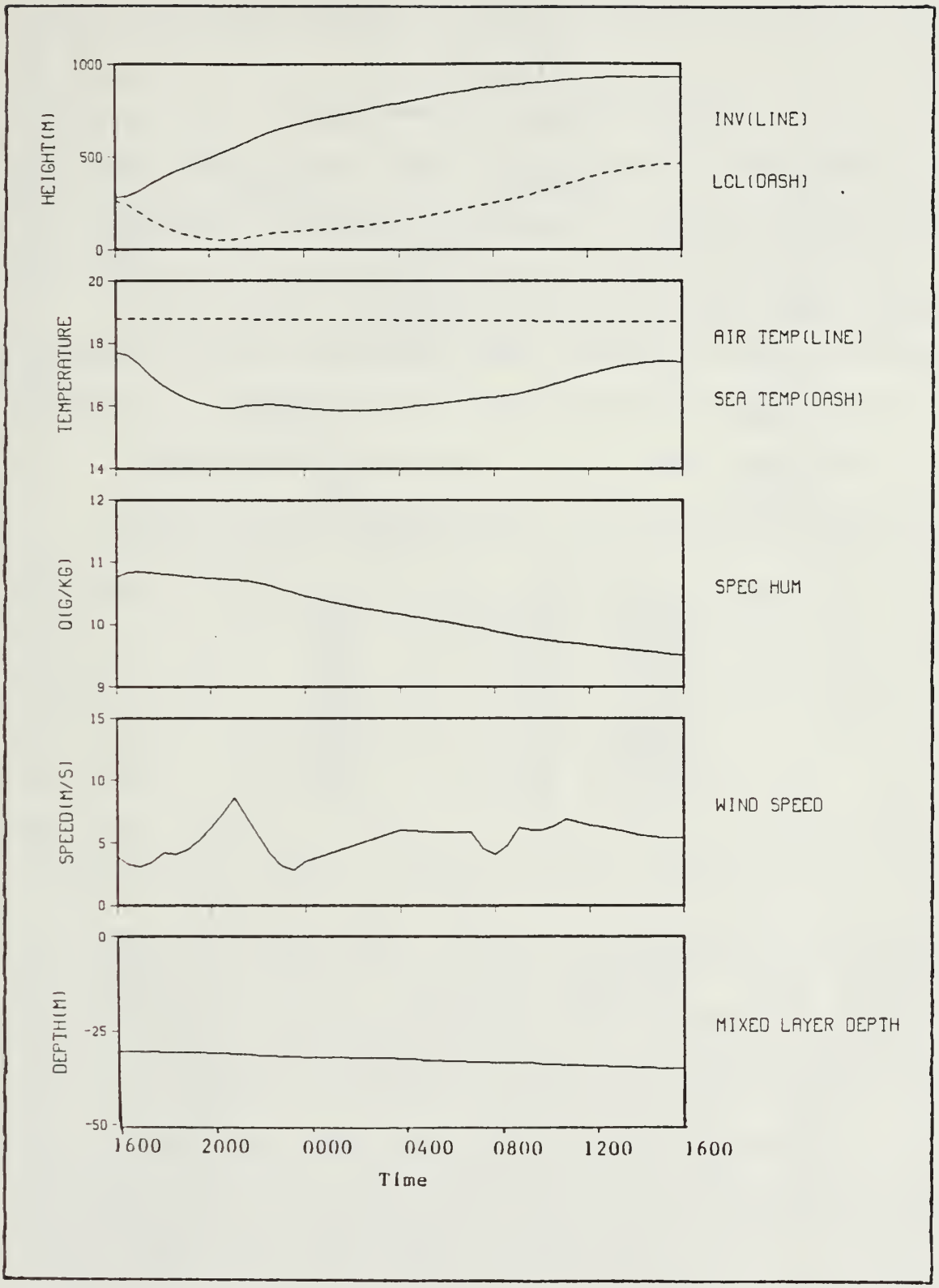

Figure 3.3 Coupled Model-Case I

TABLE I

Initialization Values-Case I

Julian Date	Sfc Pressure (mb)	Sea Sfc Temp (°C)
307	1022.4	18.78

Inversion Ht (m)	Mixed Layer Potential Temp (°C)
281	17.70

Air Temp Jump (°C)	Temp Lapse Rate (°C/m)
1.5	.0067

Spec Humidity (g/kg)	Spec Humidity Jump (g/kg m)
10.75	-.31

Spec Humidity Lps Rate (g/kg m)	LCL (m)
-.0035	849

Subsidence (m/s)	Mixed Layer Depth (m)
-.0032	30

Ocean Temp Jump (°C)	Ocean Temp Gradient (°C/m)
-.2	-.0174

Wind: Time	Speed (m/s)	Dir (°T)
1600	3.9	040
1802	4.2	319
2105	8.6	036
0017	3.5	288
0417	6.0	276
0722	5.8	293
0922	6.2	028
1123	6.9	342
1340	6.1	001
1541	5.4	340

difference is reflected in a continuous increase in moisture flux. Following sunrise, the air temperature increased associated with a decrease in specific humidity, a less rapid increase of moisture flux and an elevation of the LCL.

The inversion height increased throughout the prediction period. The time rate of change of this parameter is the difference between the rates of entrainment and subsidence. Entrainment rate reached a maximum value of 2.3 cm/s at 2130 and decreased slightly to a value of 1.5 cm/s

at the end of the period. Subsidence was held constant at a value of -.0032 m/s throughout the period. This value is representative for subsidence in this region as noted by Davidson et al., (1984). As a result, the evolution of the inversion height was dominated by the rate of entrainment. The entrainment of warm, dry air into the mixed layer also contributed to the gradual decrease of specific humidity and the increase in air temperature observed prior to sunrise.

Sea surface temperature and mixed layer depth remain constant with the uncoupled model execution i.e. no ocean variability is permitted.

2. Coupled Model

The uncoupled and coupled models predicted nearly identical atmospheric results. Clouds were present from the beginning of the period. Cloud thickness and the evolution of the LCL and inversion height remained the same as in the uncoupled model. Air temperature and specific humidity profiles were also unchanged. The coupled model determines sea surface temperature hourly. Therefore, the air-sea temperature difference, moisture and temperature fluxes would be expected to vary. In this case, the sea surface temperature decreased from an initial value of 18.78 °C to 18.69°C, a change of only .09°C. As a result, the time rate of change of moisture and temperature fluxes for the coupled and uncoupled models is nearly identical. Sea surface cooling results in convective mixing (negative buoyancy flux), cooling throughout the layer, and an increase in mixed layer depth for both the atmosphere and ocean. The impact of the ocean upon the atmospheric mixed layer processes is almost invariant in this case. The major influence upon the atmospheric mixed layer is the inversion height growth and associated entrainment.

C. OBSERVATIONS VS MODEL OUTPUT

Observed specific humidity compares favorably with model output, Fig. 3.4. The time series are nearly identical eight hours following initialization. From 12 to 18 hours after initialization the observed specific humidity shows an increase of approximately 1.0 g/kg. The model predicted a continuous decrease throughout the period. As the end of the period is approached, the model and observed specific humidity differ by less than .5 g/kg.

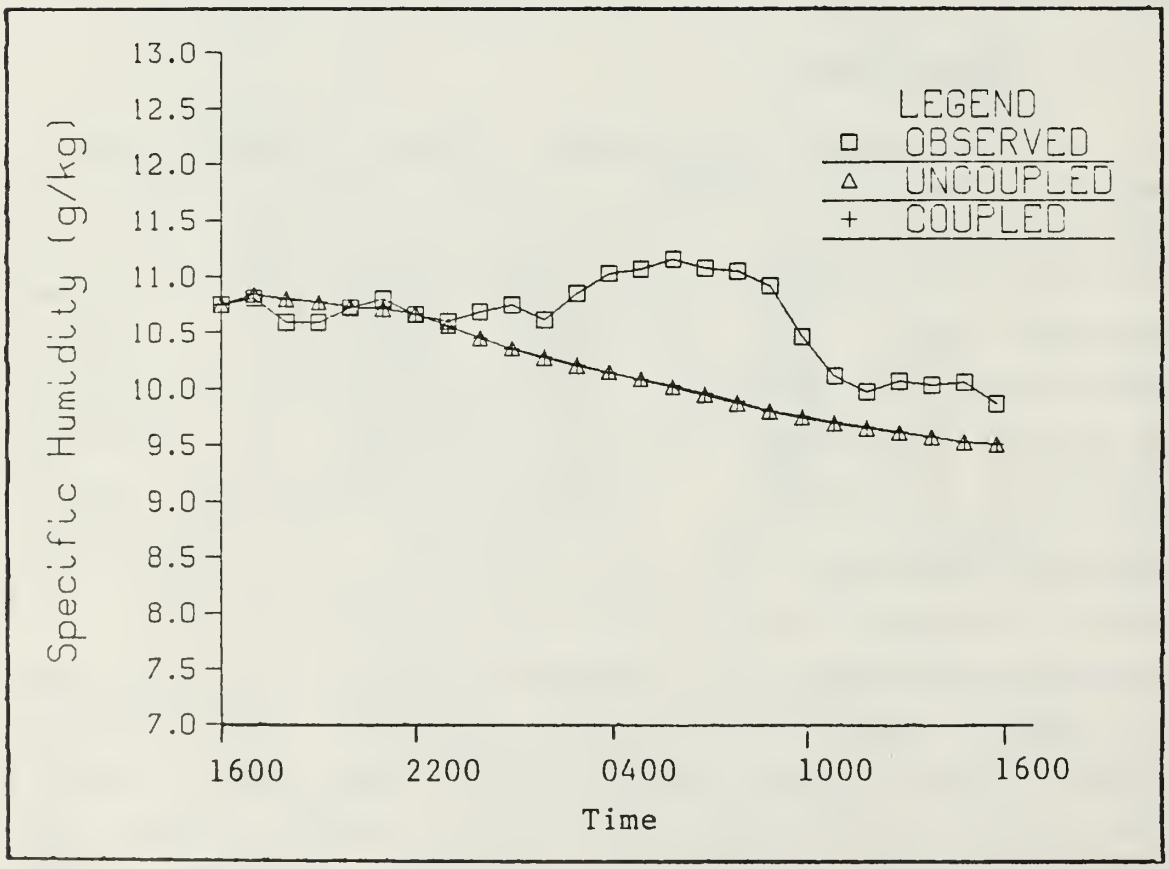

Figure 3.4 Specific Humidity Observed vs Model (Case I)

The model prediction of air temperature differs by as much as 2°C from observed values from 2000 to 0400, Fig.

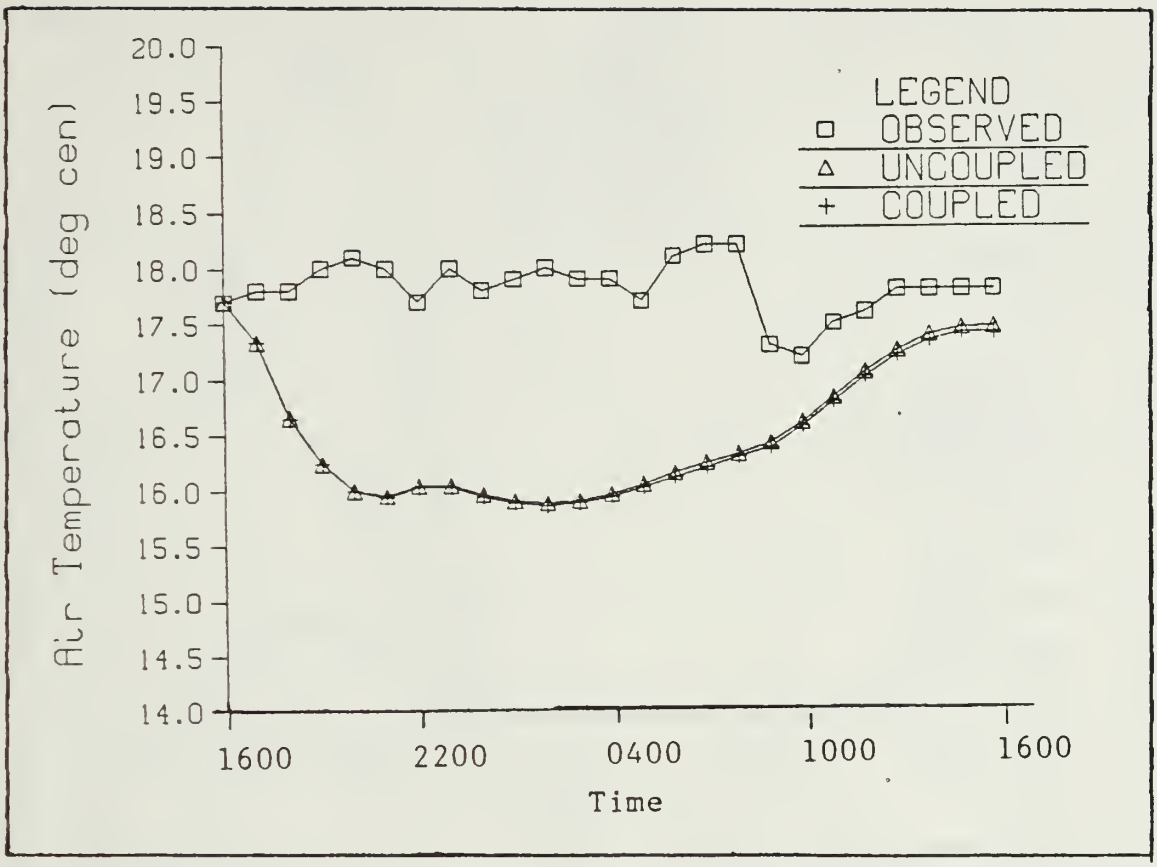

Figure 3.5 Air Temperature
Observed vs Model (Case I)

3.5. From 1000 to the end of the period, the observations and predictions demonstrated an increase and eventually attained a constant air temperature, differing by less than 0.5°C. The large difference in air temperature (ca. 2°C) which occurs was a result of thick cloud cover and resultant shortwave radiation deficit.

There were vast differences in observed and modeled shortwave radiation, Fig. 3.6. The radiation for a cloud free case verifies that there was a cloud cover present. This result is deduced from the difference in shortwave radiation between the cloud free case and the observed values. Clouds were present from 15 to 20 hours after

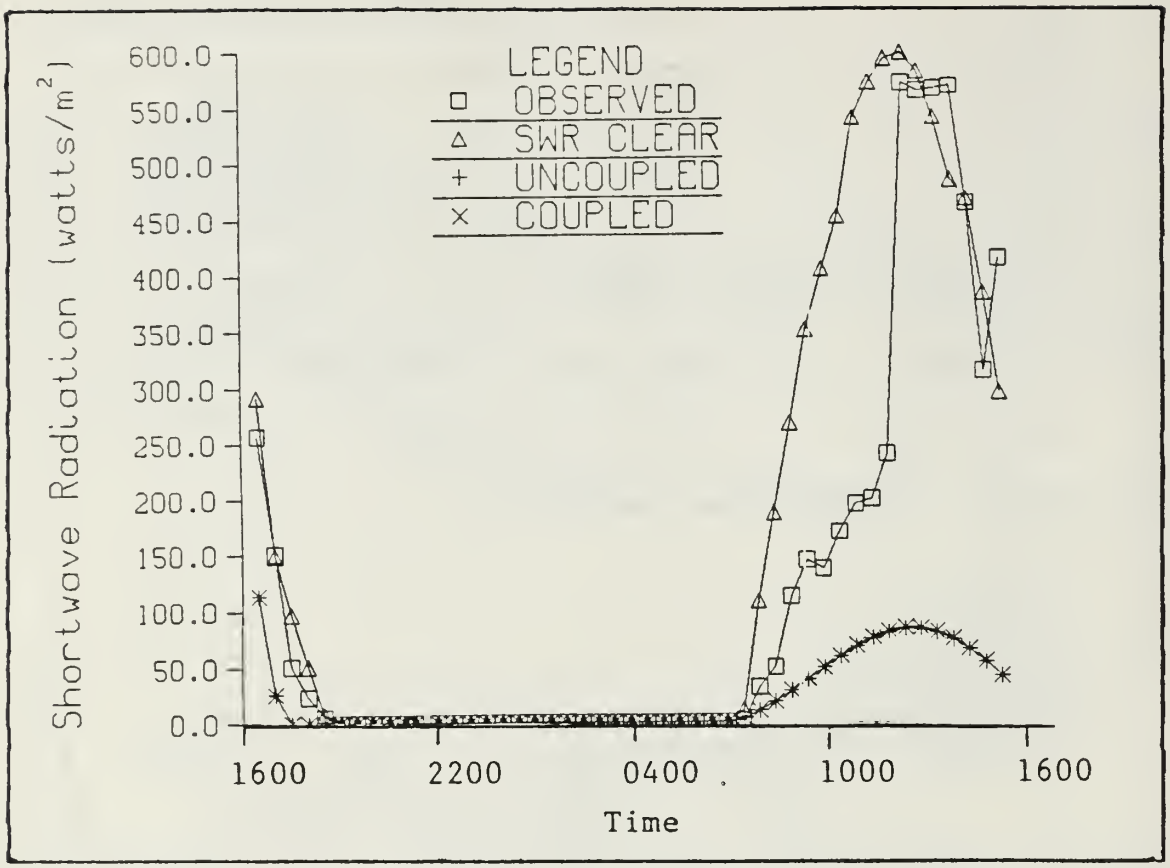

Figure 3.6 Shortwave Radiation Observed vs Model (Case I)

initialization. Uncoupled and coupled model calculations of shortwave radiation are closely correlated. However, they are substantially smaller than the observed values. This difference is a result of the assumption of complete cloud cover when the LCL is beneath the inversion height. Horizon to horizon cloud cover will result in a fractional amount of shortwave radiation in comparison with a variable amount of cloud cover.

The effect of the over prediction of cloud cover has been addressed previously. The cooler air temperature determined by the model and the cooling of the sea surface and deepening of the mixed layer by the coupled model are two examples. These differences impact variables such as

specific humidity and LCL, which are functions of air temperature. These variables are fundamental to the determination of the rate of change of all of the model parameters.

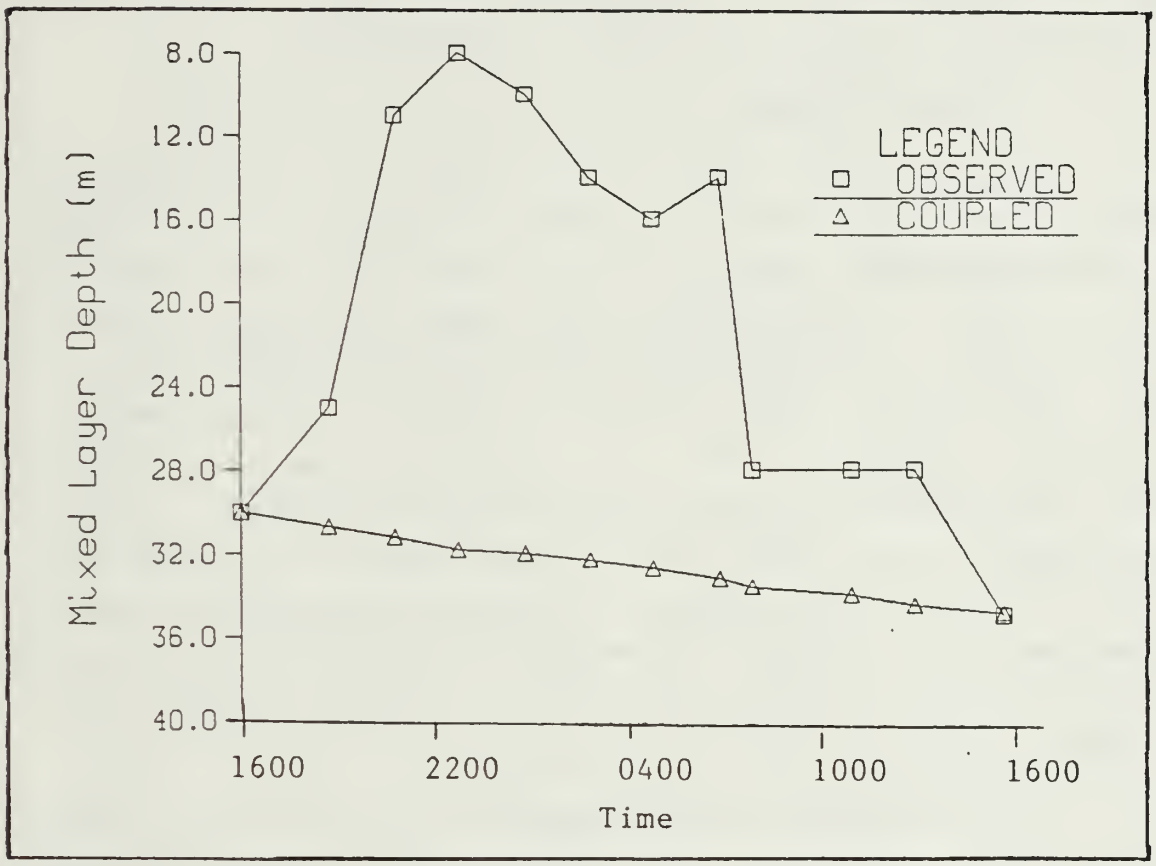

Figure 3.7 Mixed Layer Depth
Observed vs Model (Case I)

Observations indicated a shallowing of the mixed layer from 1900 through 2300, Fig. 3.7. This was followed by a gradual deepening. It is due tc the surface heating and the distribution of heat by wind mixing followed by radiative cooling and convective overturning. The model predicted a continuous deepening of the mixed layer due to the substantially reduced values of shortwave radiation and the resultant sea surface cooling and convective instability.

D. CASE II: 1554 PDT 04 NOVEMBER-1600 05 NOVEMBER 1983

The initializing variables for the second 24 hour period are listed in table II. Uncoupled and coupled model outputs are presented in Figs. 3.8 and 3.9 respectively.

1. Uncoupled Model

In this case, (Fig. 3.8), the cloud development is less extreme than that which arose in Case I. A cloud of minimum thickness formed when the model was initiated (20 m). As the run progressed, the model determined a fairly constant LCL, whereas inversion height increased rapidly from 1600 through 1900 (492 to 768 m). The inversion attained a height of 1093 m at 0630 and remained at this level until 1030, at which time it began to lower. At the conclusion of the model run the inversion had dropped 23 m from its maximum of 1093 m. The LCL decreased slightly throughout the period. It began at a level of 472 m and reached a final height of 422 m. The cloud thickness had a maximum of 701 m at 0930, 05 November.

The behavior of the inversion is reflected in the modeled entrainment rate. As the inversion height increased in the early portion of the period, entrainment rate attained an absolute maximum value of 3.68 cm/s. Thereafter, the predicted rate of entrainment decreased, ultimately attaining a value of .679 cm/s. The final value represented an absolute minimum. Since the prescribed subsidence rate was held constant, the rate of entrainment again dominated the evolution of the inversion height.

The LCL remained relatively constant throughout. This was a result of the compensating effects of dry air entrainment and an increasingly larger air-sea temperature

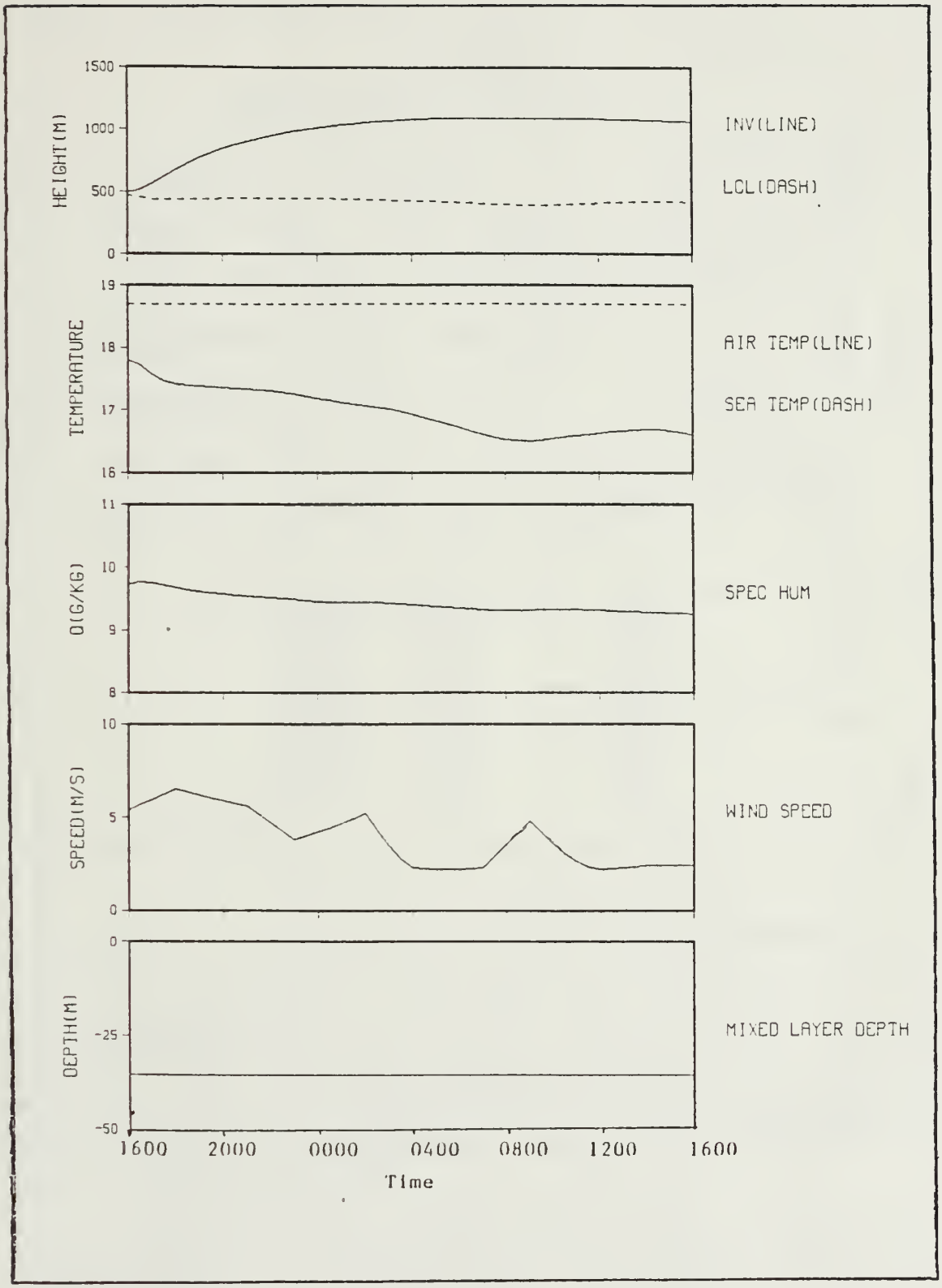

Figure 3.8 Uncoupled Model-Case II

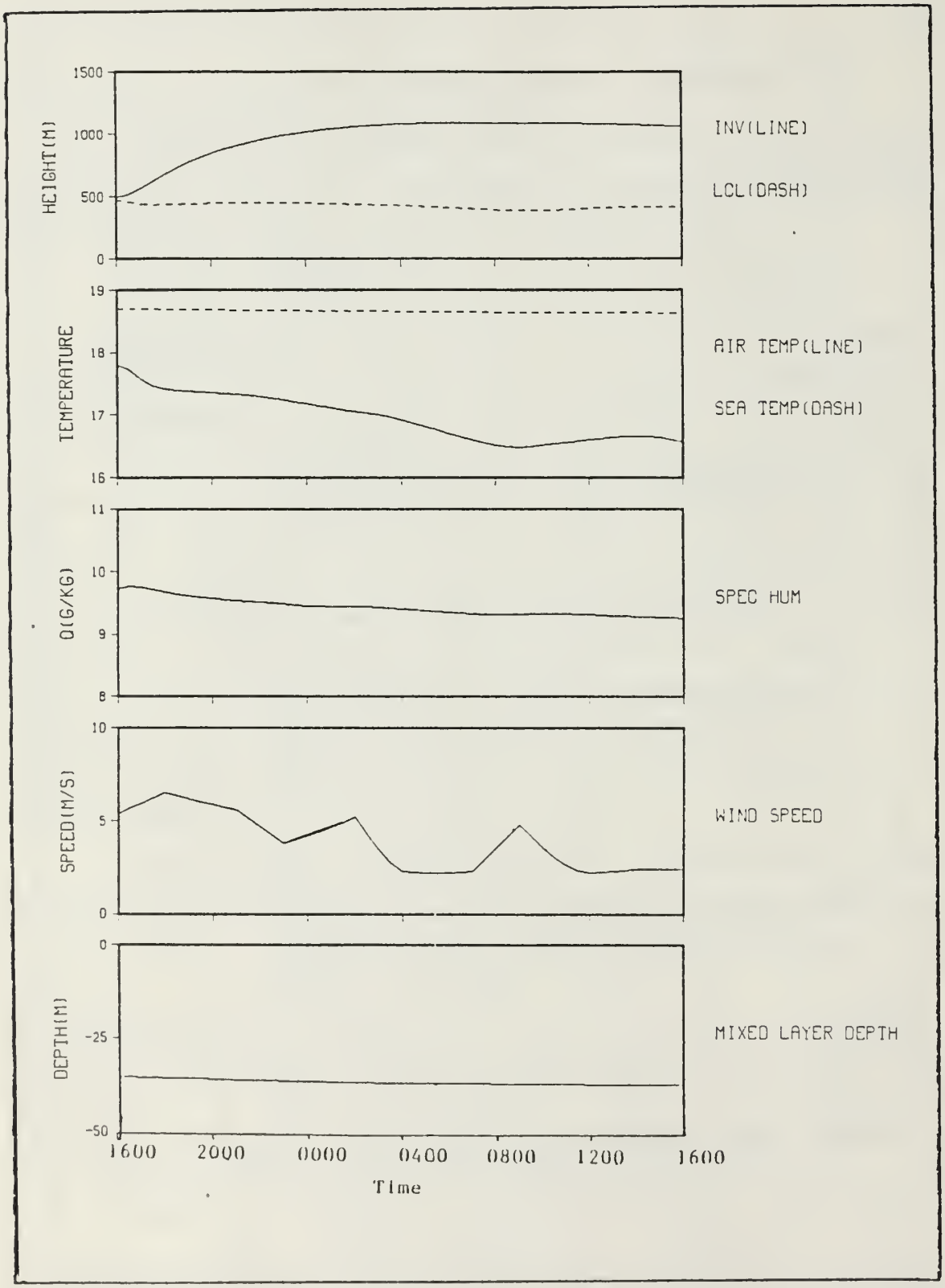

Figure 3.9 Coupled Model-Case II

TABLE II

Initialization Values-Case II

Julian Date	Sfc Pressure (mb)	Sea Sfc Temp (°C)
308	1022.3	18.70

Inversion Ht (m)	Mixed Layer Potential Temp (°C)
492	17.80

Air Temp Jump (°C)	Temp Lapse Rate (°C/m)
1.5	.0065

Spec Humidity (g/kg)	Spec Humidity Jump (g/kg m)
9.72	-.94

Spec Humidity Lps Rate (g/kg m)	LCL (m)
-.0017	1079.12

Subsidence (m/s)	Mixed Layer Depth (m)
-.0039	35

Ocean Temp Jump (°C)	Ocean Temp Gradient (°C/m)
-.2	-.1411

Wind: Time	Speed (m/s)	Dir (°T)
1600	5.4	340
1830	6.5	340
2100	5.6	351
2330	3.8	345
0200	5.2	325
0430	2.3	016
0700	2.3	344
0930	4.8	333
1200	2.2	270
1430	2.4	265

difference. The former would force an increase in the LCL, the latter a decrease. This balance is also evident in the nearly constant predicted specific humidity values. As the moisture flux into the layer increased (due to the increasing air-sea temperature difference) the incorporation of dry, warm air (entrainment) resulted in a slight variation in specific humidity.

Air temperature in the mixed layer, if viewed in terms of radiative heating and cooling, would be expected to decrease after sunset and increase after sunrise. This is

the case as shown in Fig. 3.8. The modeled shortwave radiation is again underestimated. As a result, a significant decrease in air temperature occurred through 16 hours into the period due to cloud top long wave radiation.

2. Coupled Model

As observed in Case I, the coupled and uncoupled model predictions are essentially identical in this case. The coupled model prediction demonstrated a decrease in sea surface temperature and a deepening of the mixed layer. Sea surface temperature decreased from 18.7 to 18.63 °C. The moisture flux decrease, due to the reduced sea temperature, was too small to force any appreciable change in specific humidity or LCL. The deepening of the mixed layer from an initial depth of 35 to a 37.4 m had no effect upon the atmospheric boundary layer.

While Case I and Case II experienced similar decreases in sea surface temperature, the former deepened the mixed layer by a factor of two greater than the latter. However, friction velocity was larger in Case I than Case II. Therefore, the variation of the mixed layer depth was in response to wind forcing.

3. Observations vs Model Predictions

The predicted and observed specific humidity were significantly different, Fig. 3.10. There is no difference between coupled and uncoupled predictions as they exhibit a slight decrease throughout the period. Observed specific humidity varied in a cyclical fashion due to the relative humidity variation.

Values of specific humidity were calculated externally using air temperature, pressure and relative humidity. Unlike Case I, a large decrease in relative humidity was

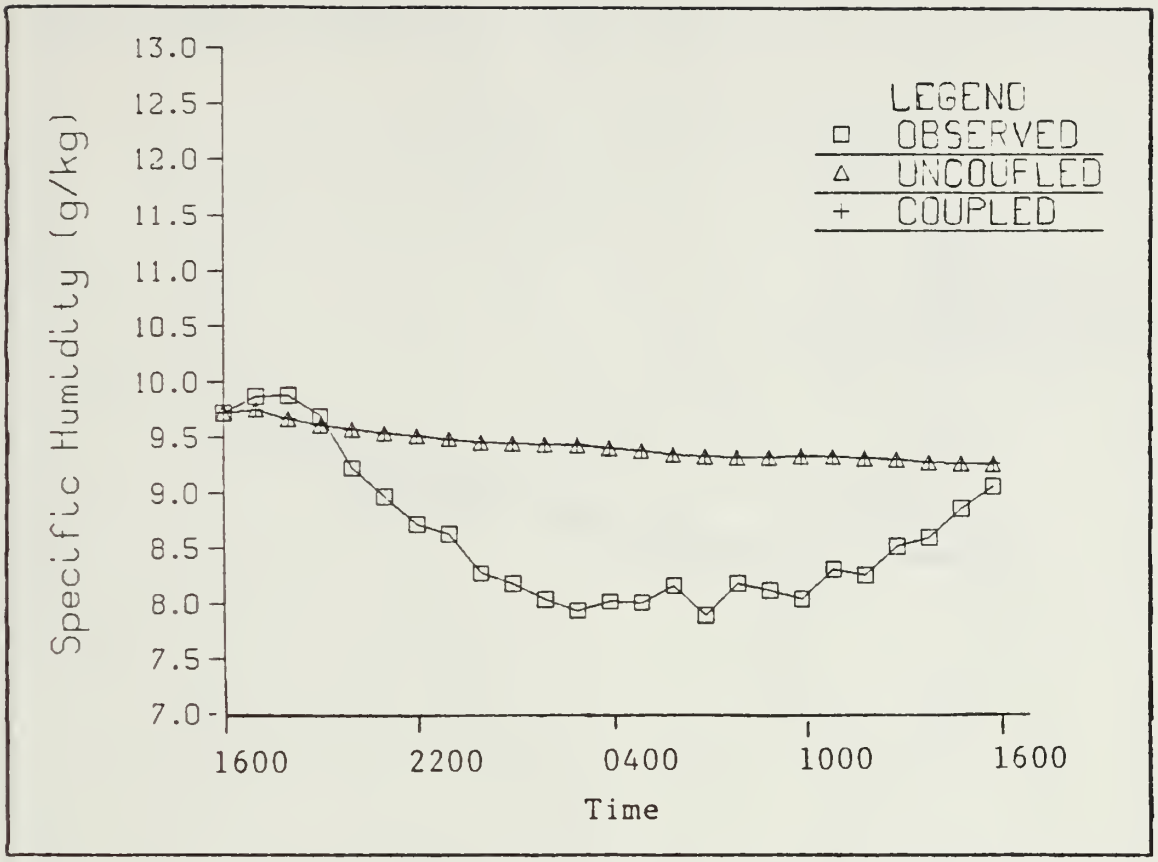

Figure 3.10 Specific Humidity
Observed vs Model (Case II)

experienced. Specific and relative humidity changes are forced by surface moisture flux and entrainment. Since the predicted and observed values for air and sea surface temperature are nearly the same, the difference lies in the entrainment. As noted earlier, the predicted rate of entrainment decreased through the period. Actual entrainment must have increased during the middle of the run and decreased at the end.

The radiosonde data (Fig. 3.11) support the observed decrease in mixed layer specific humidity. Mixed layer specific humidity begins at a value of 9.76 g/kg, decreased to 7.84 g/kg 16 hours later, and attained a value of 8.98

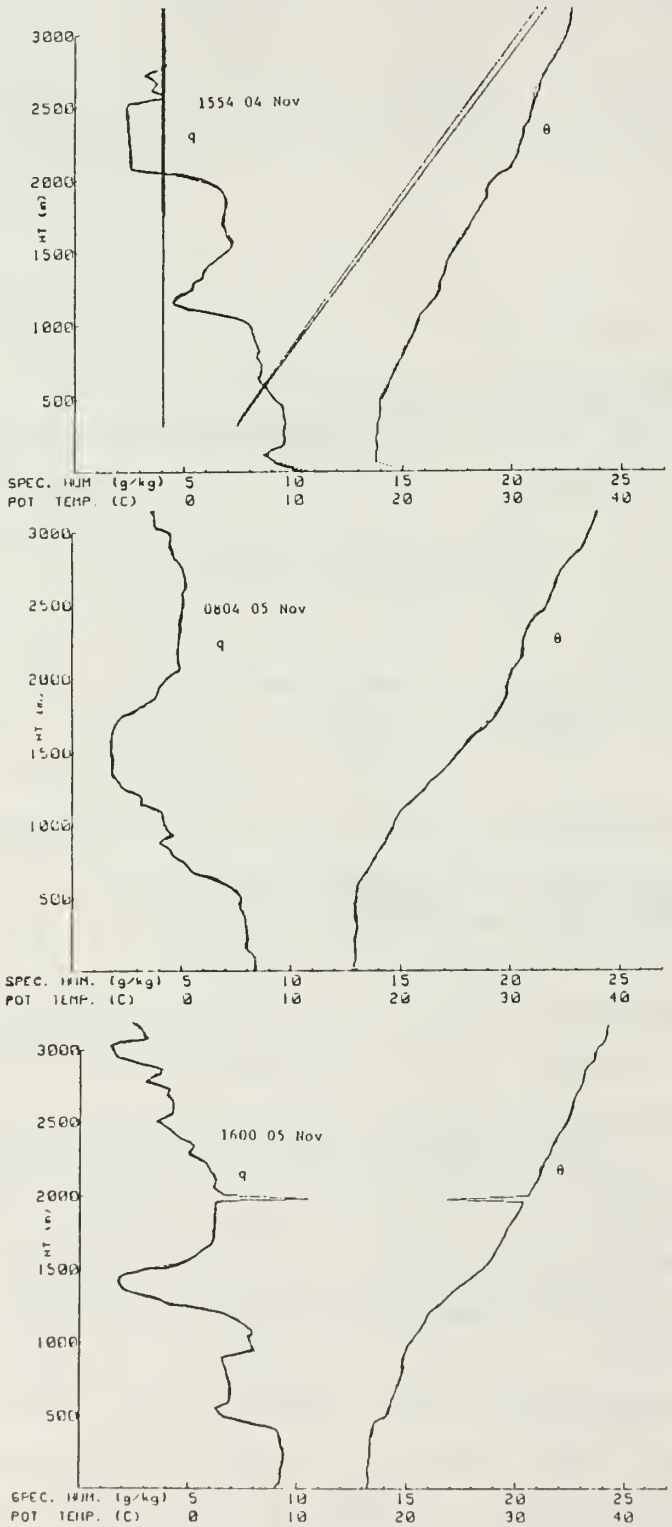

Figure 3.11 Radiosonde Profiles

g/kg 24 hours into the period. The predicted entrainment is, therefore, smaller than that observed.

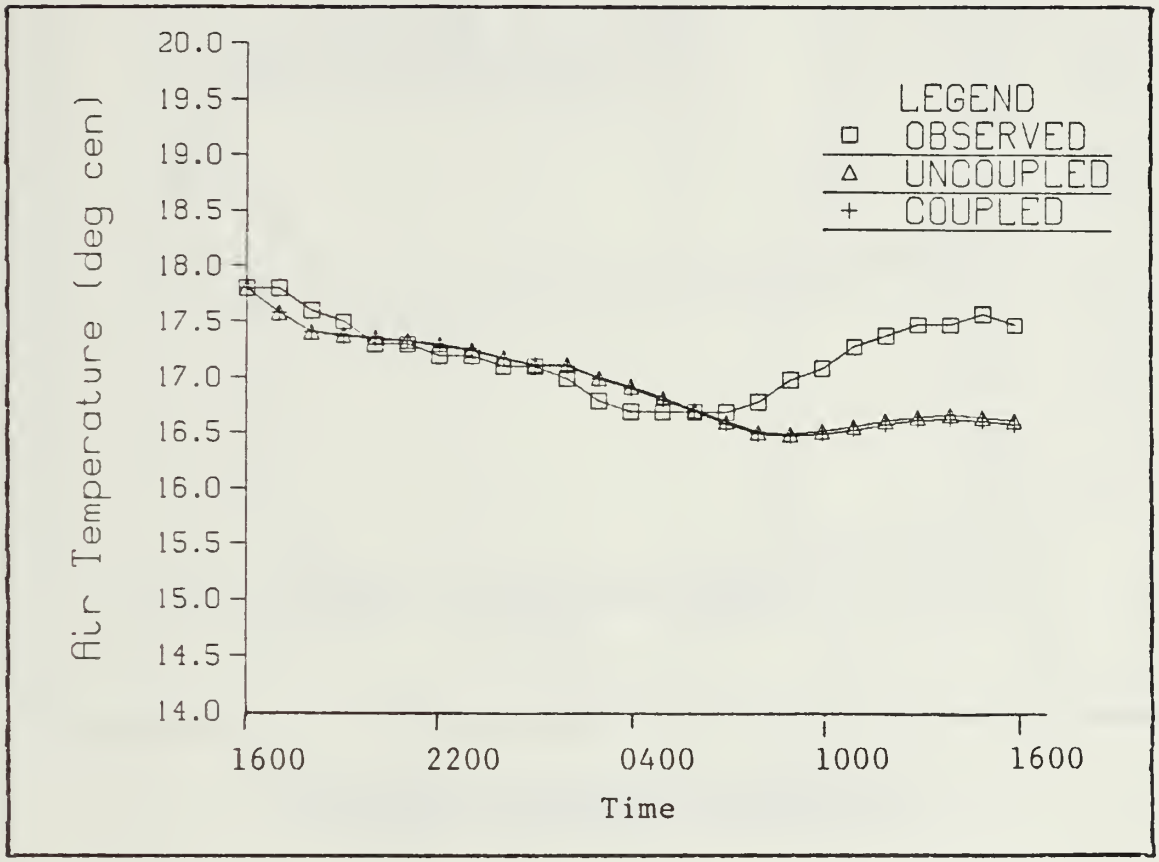

Figure 3.12 Air Temperature
Observed vs Model (Case II)

The air temperature was in close agreement for observed, uncoupled and coupled cases exists 16 hours into the period, Fig. 3.12. From this time, the predicted values increase slightly while the observed air temperature increases by greater than 0.5°C. At the end of the period a temperature difference of 0.86°C exists.

Predicted sea surface temperature agrees with observed values 20 hours into the run, Fig. 3.13. The observed sea surface temperature increased 0.3°C from 16 to

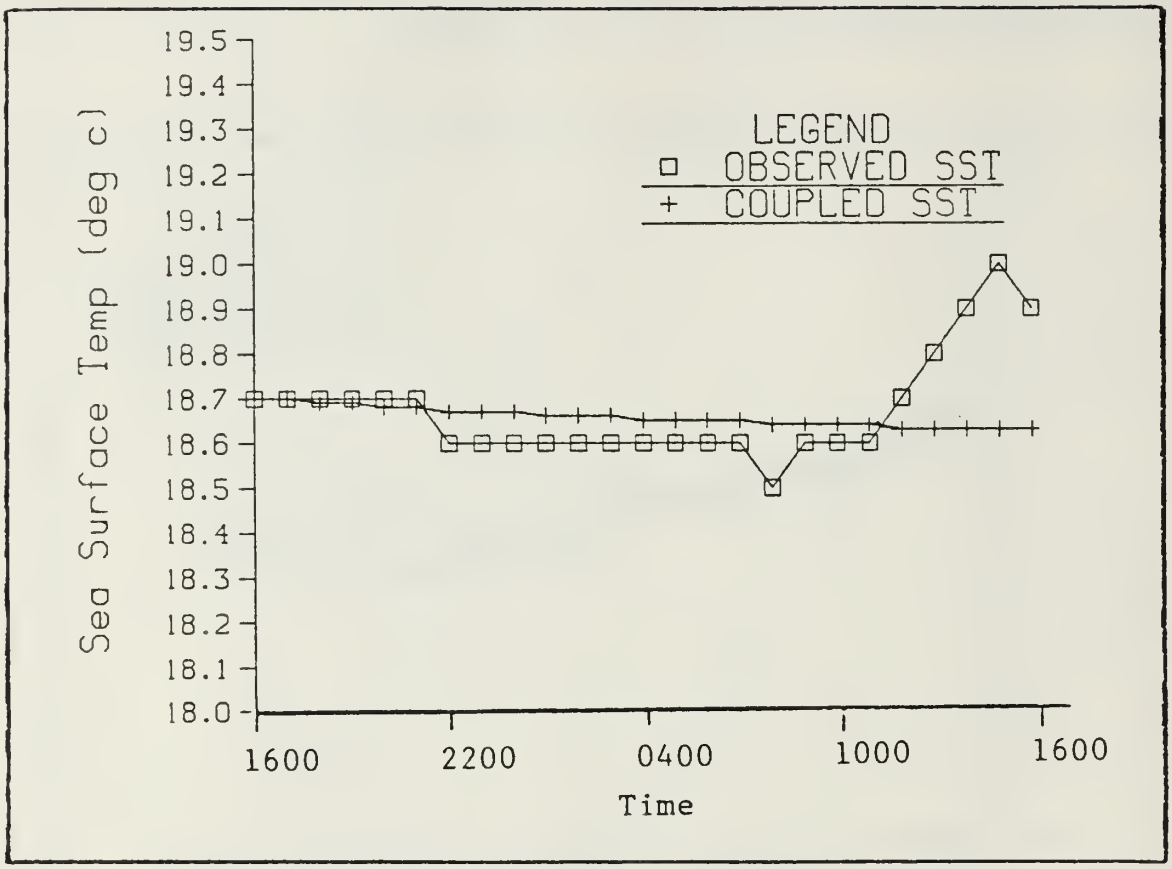

Figure 3.13 Sea Surface Temperature Observed vs Model (Case II)

24 hours after initialization (1200 to 1600 local time) due to shortwave radiative heating. Predictions fail to demonstrate this increase due to the extensive cloud cover and associated shortwave radiation deficit. This dichotomy is absent in the early stages of the run since the model was initialized with the observed sea surface temperature.

Shortwave radiation is again underestimated, Fig. 3.14. A clear sky was observed as depicted by the agreement of observed and clear sky values of shortwave radiation. The model predicted a thick cloud layer and assumed horizon to horizon coverage. This prediction resulted in a severe underestimation of shortwave radiation at the sea surface.

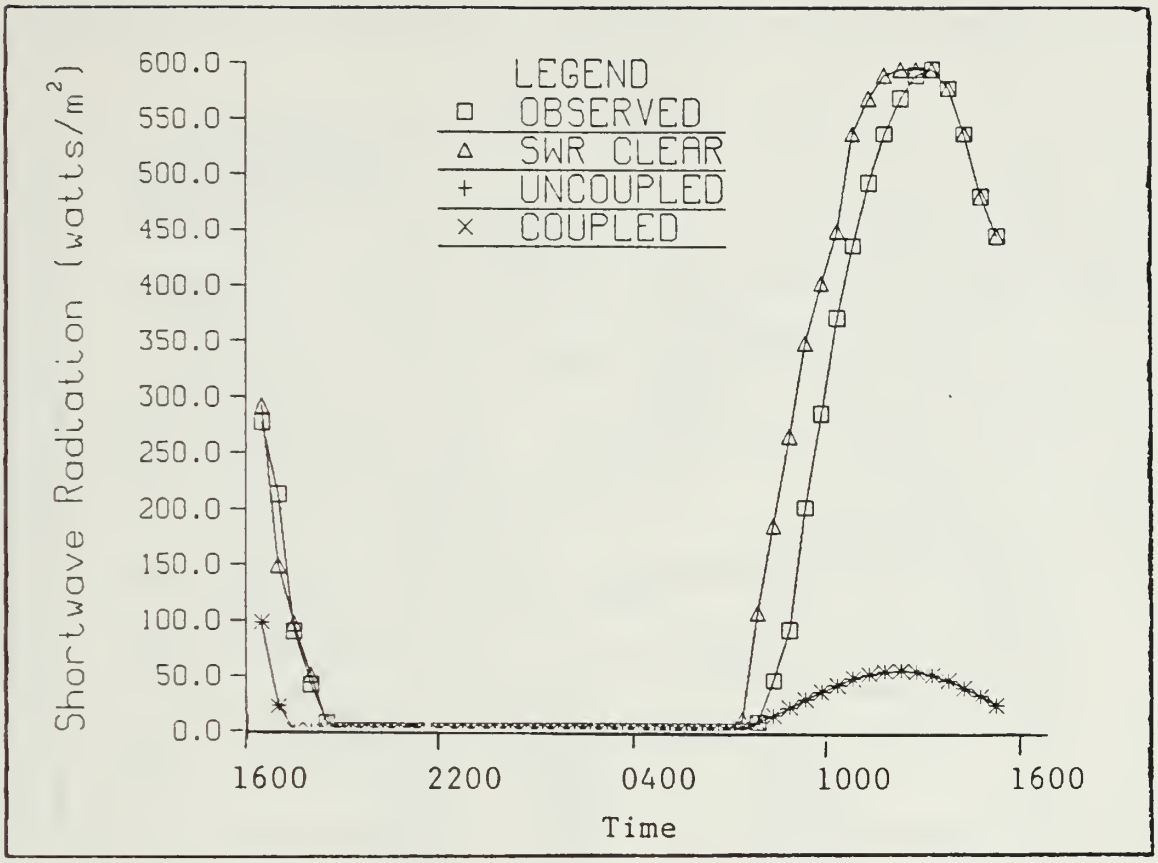

Figure 3.14 Shortwave Radiation Observed vs Model (Case II)

As in Case I, the effects of this radiation deficit are wide ranging throughout the model.

Through the comparison of coupled model and observed variations of the mixed layer depth, a periodic retreat of the mixed layer was observed, Fig. 3.15. A minimum depth was attained eight to ten hours after the maximum in shortwave radiation due to the delayed oceanic response to heating and the relatively light winds forcing the mixing. Additionally, the effects of tides and internal waves are most likely present as evidenced by the periodic variation in mixed layer depth. The shortwave radiation deficit forced a deepening of the mixed layer, which resulted from

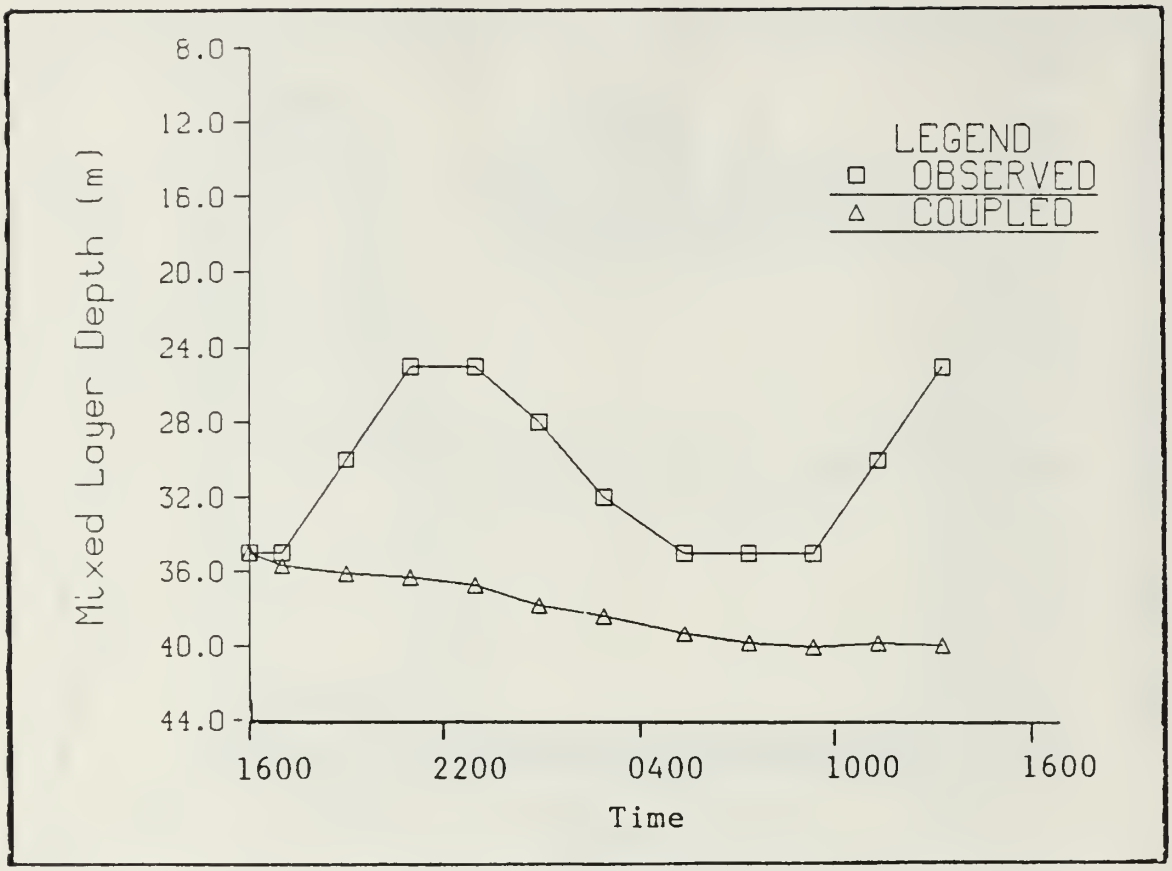

Figure 3.15 Mixed Layer Depth
Coupled vs Model

cooling of the sea surface and convective mixing. This pattern corresponds to the remainder of the modeled variables. However, it is significantly different than the response of the ocean to the atmospheric forcing.

E. CASE III: 1600 03 NOVEMBER-1600 05 NOVEMBER 1983

To compare model performance and observations for a period greater than 24 hours, a 48 hour period was selected. Due to the limitations imposed upon the experiment by the environment and equipment malfunction, the time frames for Cases I and II were combined to provide the longer forecast

TABLE III

Initialization Values-Case III

Julian Date	Sfc Pressure (mb)	Sea Sfc Temp (°C)
308	1022.4	18.69

Inversion Ht (m)	Mixed Layer Potential Temp (°C)
928	17.41

Air Temp Jump (°C)	Temp Lapse Rate (°C/m)
10.3	.0065

Spec Humidity (g/kg)	Spec Humidity Jump (g/kg m)
9.52	-3.8

Spec Humidity Lps Rate (g/kg m)	LCL (m)
-.0017	417

Subsidence (m/s)	Mixed Layer Deptn (m)
-.0032	34

Ocean Temp Jump (°C)	Ocean Temp Gradient (°C/m)
-.2	-.1411

Wind: Time	Speed (m/s)	Dir (°T)
1600	5.4	340
1830	6.5	340
2100	5.6	351
2330	3.8	345
0200	5.2	325
0430	2.3	016
0700	2.3	344
0930	4.8	333
1200	2.2	270
1430	2.4	265

period. The output variables from the last time step of Case I were employed as initializing variables for the second 24 hour period of Case III. These variables are listed in Table III.

The most obvious difference in the Case III prediction as compared with that of Case II was that there were no rapid changes in the predicted variables, Figs. 3.16 and 3.17. The most obvious difference in the Case III prediction as compared with that of Case II was that there

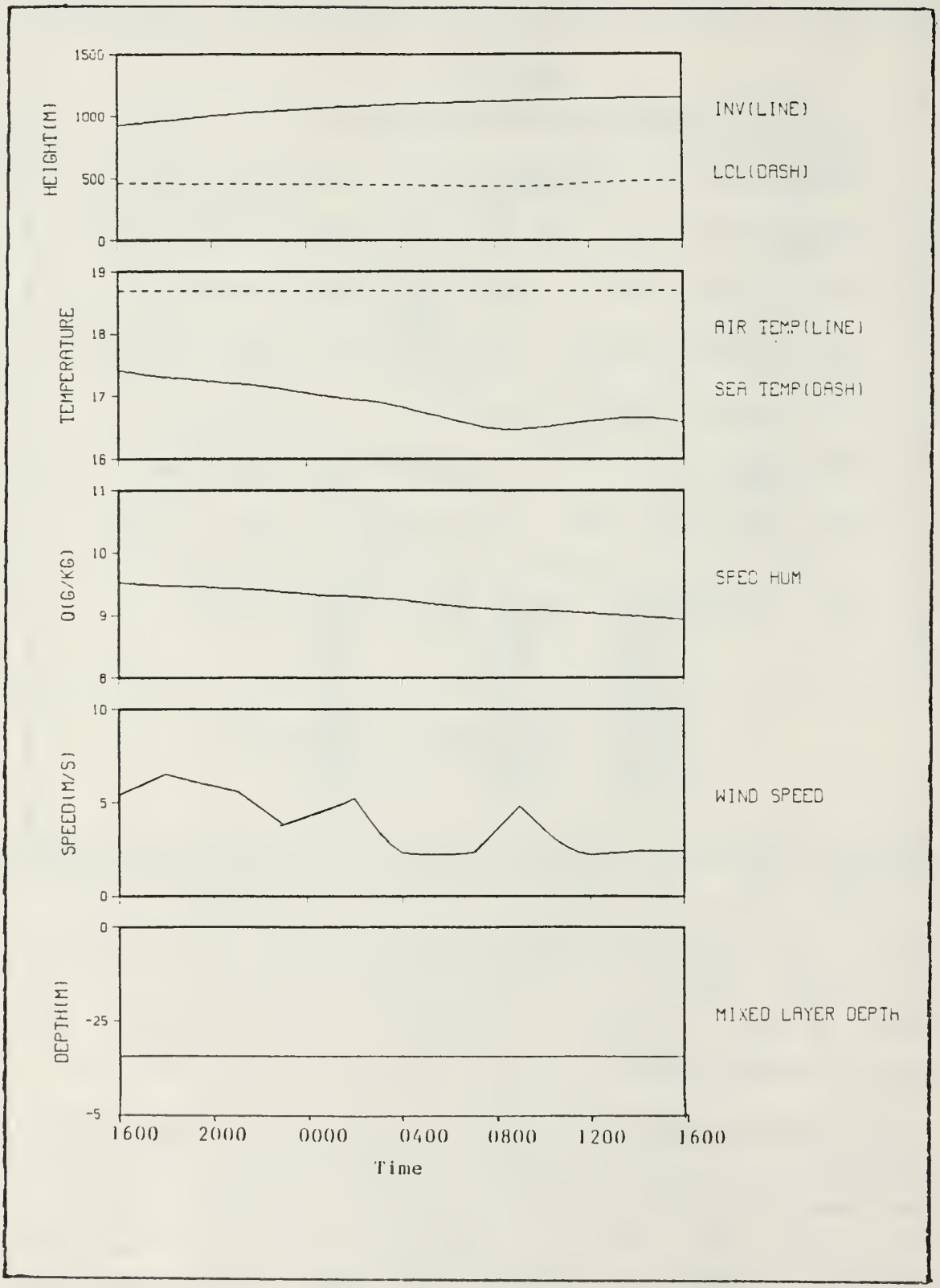

Figure 3.16 Case III Uncoupled Model

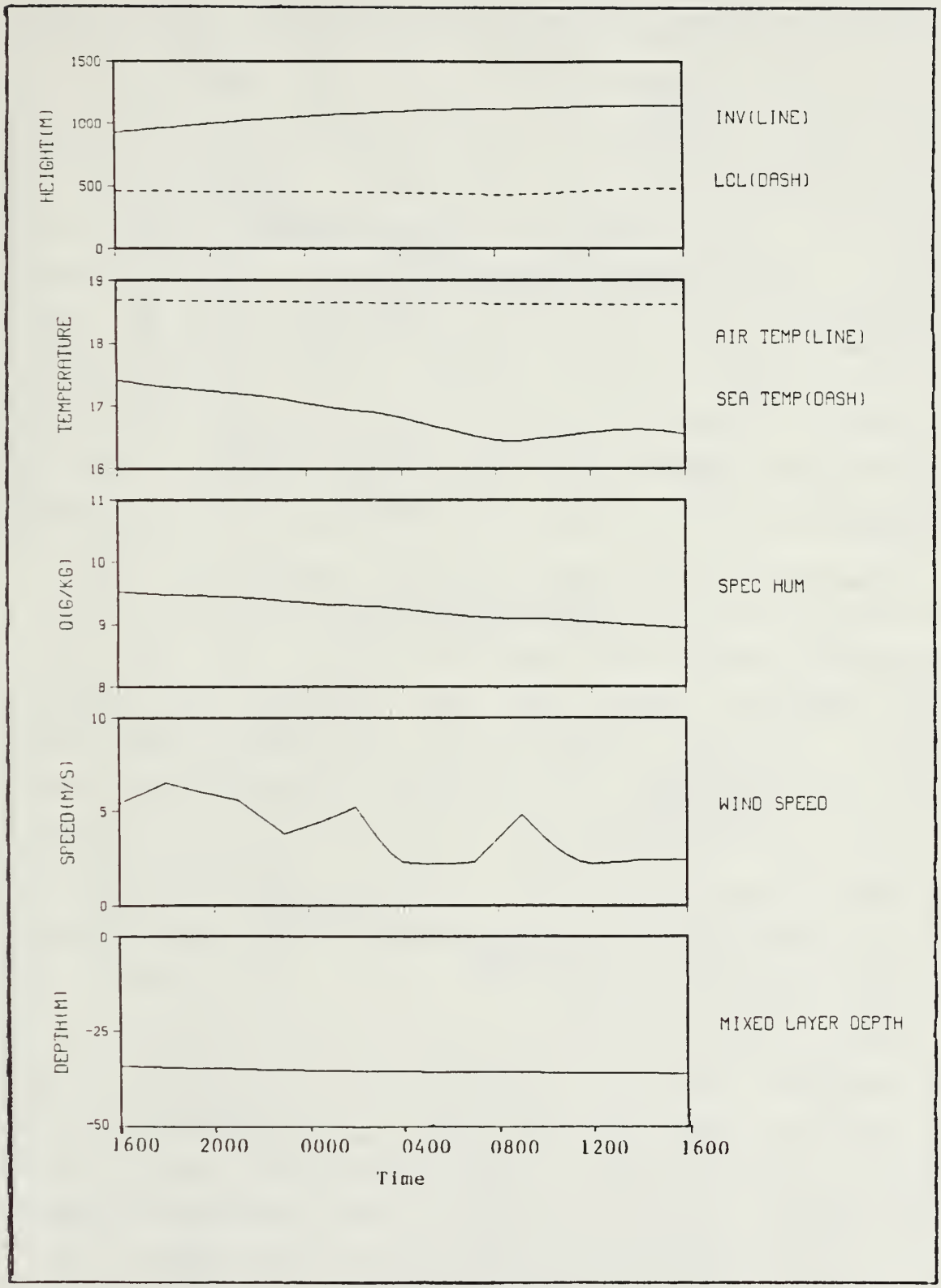

Figure 3.17 Case III Coupled Model

were no rapid changes in the output variables. The inversion height increased gradually from an initial value of 928 m to a final value of 1146 m. The LCL ranged from an initial value of 464 m to a minimum value of 438 m to a final height of 483 m. The LCL and inversion height attained final values of 424 and 1073 m, respectively, in Case II. Cloud thickness changed slightly during the period. It began at 464 m and increased to 663 m. Cloud thickness for Case II grew to a thickness of 649 m. The radiosonde soundings for the latter 24 hours period of Case III (Fig. 3.11) revealed the height of the inversion to be increasing. Though the profiles are not ideal, the final inversion base height is of the order of 1000 m. Hence, fairly good agreement exists for Cases II and III in this regard.

Temperature also varied gradually during the period. Both Cases II and III demonstrated a diurnal variation. Air temperature profiles are depicted in Figs. 3.18 and 3.19. Close agreement exists from the uncoupled and coupled models. There is essentially no difference between the output for these cases. The shortwave radiation deficit and associated lack of heating was obvious from 16 to 24 hours into the runs. An agreement of temperature values at the beginning of each run occurred as the result of initialization and because the runs began at 1600. Darkness occurred shortly thereafter. Thus there was a minimal amount of shortwave radiative heating.

A very close agreement in specific humidity resulted for both uncoupled and coupled models, and for the 24 and 48 hour periods, Figs. 3.20 and 3.21. As highlighted in the discussion of Case II the difference between observed and modeled specific humidities was due to an apparent increase in the actual rate of entrainment of warm dry air into the mixed layer, while modeled entrainment remained fairly constant and smaller in magnitude.

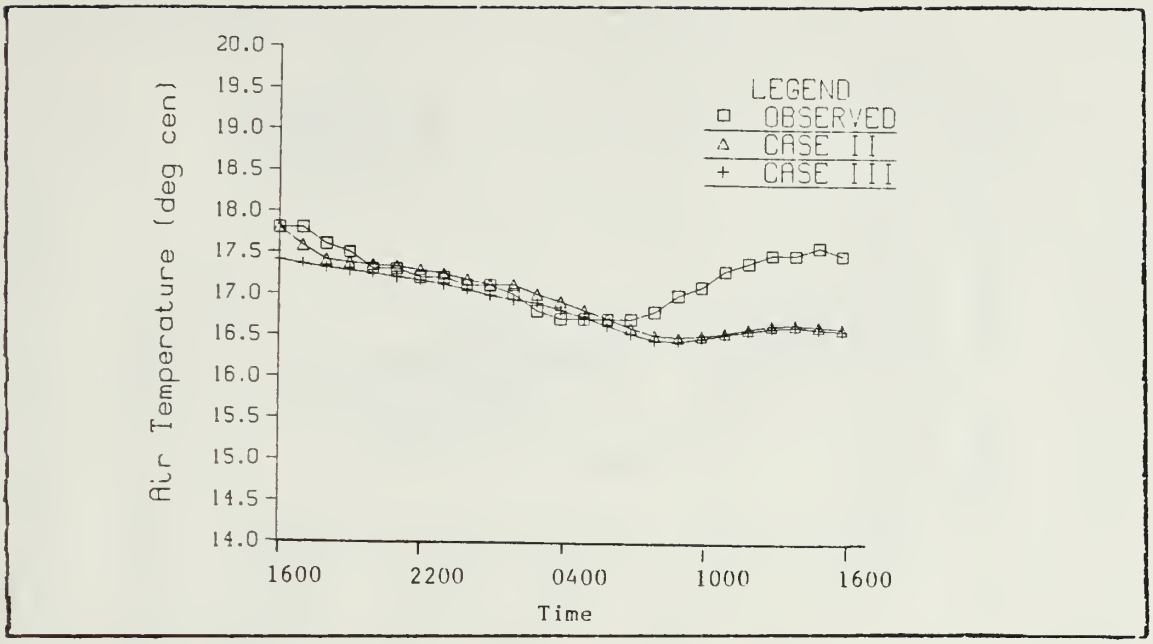

Figure 3.18 Air Temperature Comparison Uncoupled Models

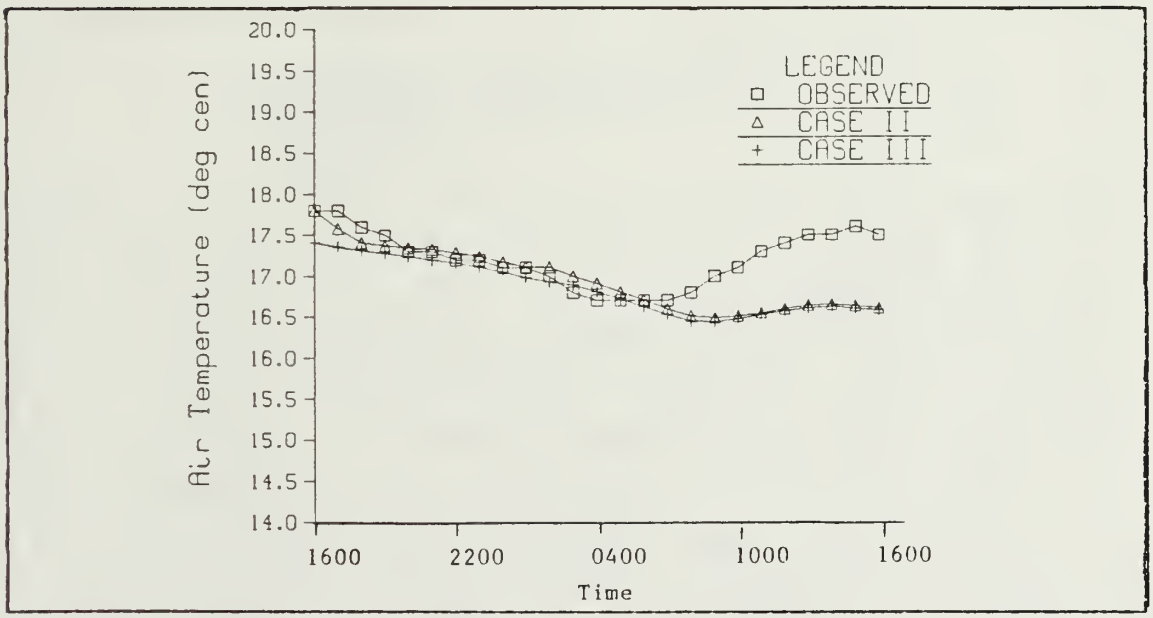

Figure 3.19 Air Temperature Comparison Coupled Models

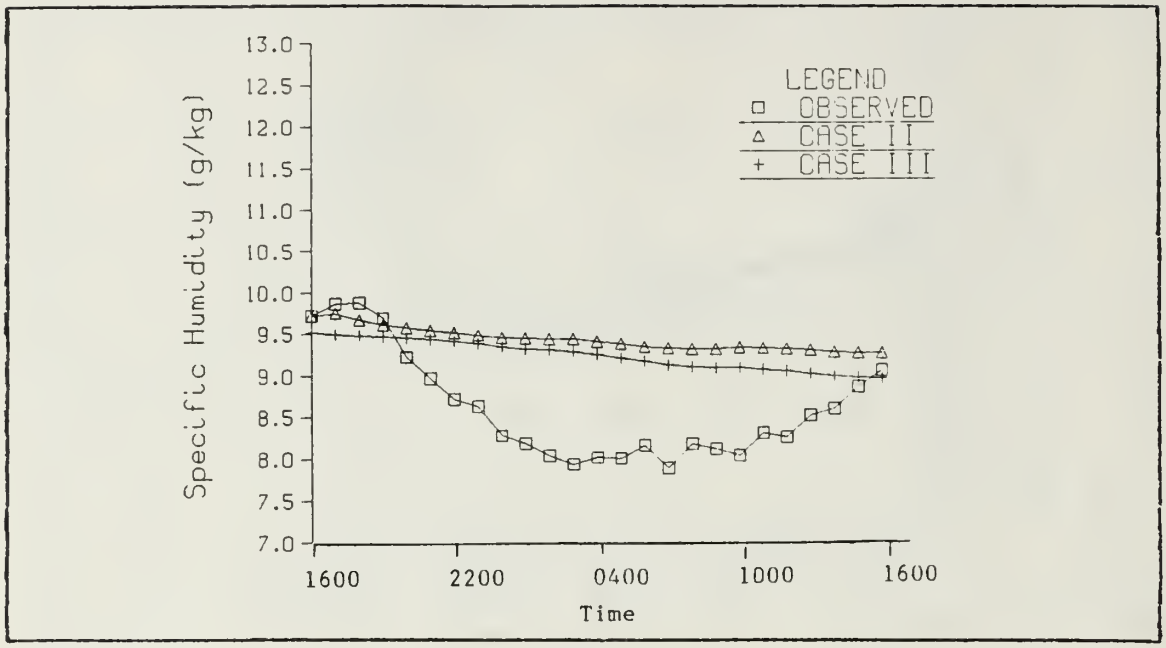

Figure 3.20 Specific Humidity
Uncoupled Model

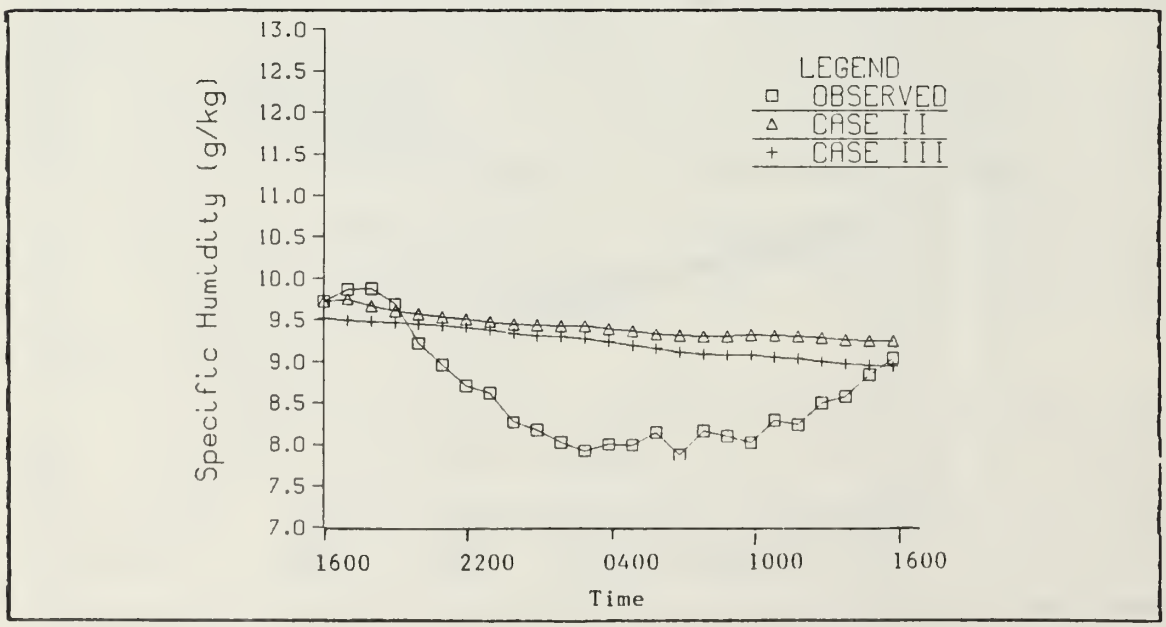

Figure 3.21 Specific Humidity
Coupled Model

Shortwave radiation varied as expected for the 48 hour period, including the latter 24 hours, Figs. 3.22 and 3.23. The order of magnitude of the difference between observed and modelled values has been the same for the three cases

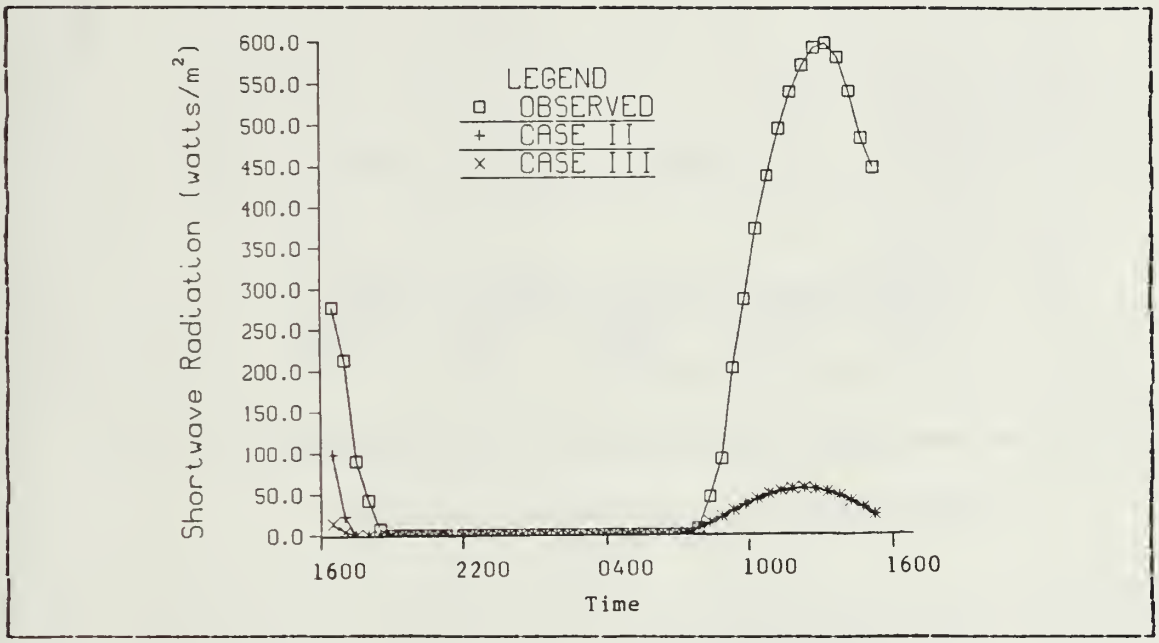

Figure 3.22 Shortwave Radiation
Uncoupled Model

analyzed. As in Cases I and II, the extreme cloud cover and minimal shortwave radiation have forced significant differences in modeled variables. The impact of the predicted radiation deficit was obvious in the behavior of air temperature in Case III and was also evident in the difference between observed and modeled mixed layer depth and sea surface temperature.

While the mixed layer deepens in Cases II and III, the observed mixed layer depth responds as expected to surface heating and wind mixing, Fig. 3.24. As described in Cases I and II, an eight hour lag exists between maximum shortwave radiation and maximum retreat of the mixed layer, which

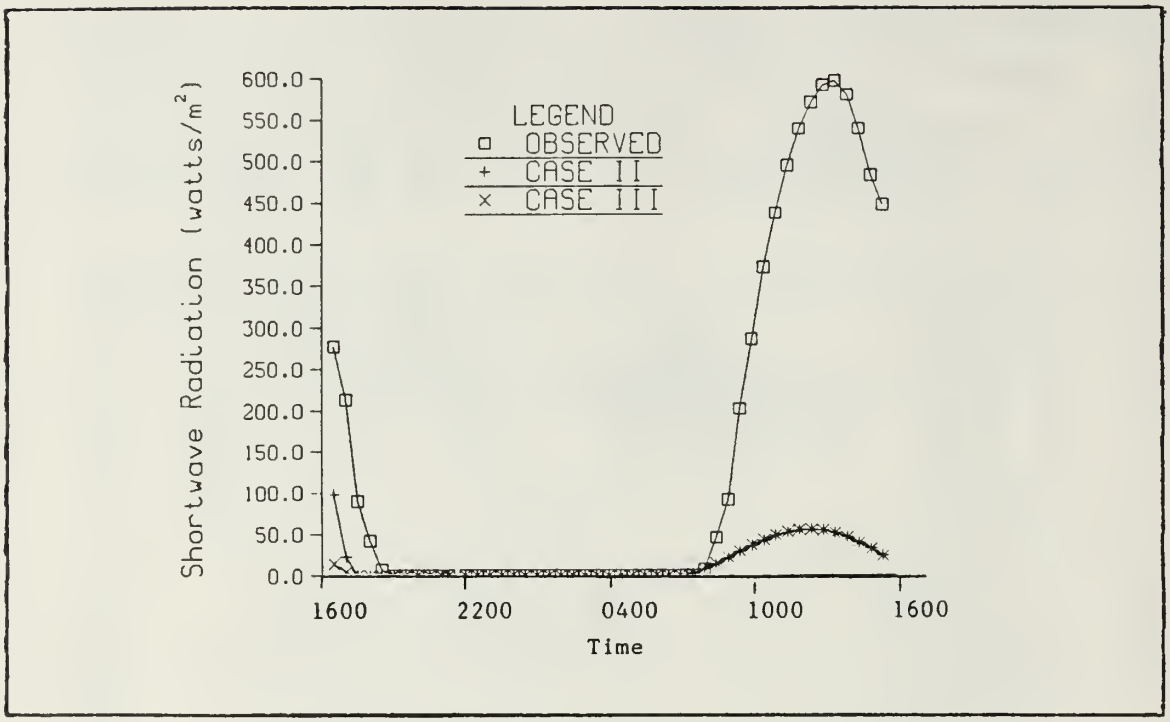

Figure 3.23 Shortwave Radiation Coupled Model

results from the relatively slow response of the ocean to atmospheric thermal forcing.

The modeled cooling of the sea surface temperature in all cases is yet another effect of the shortwave radiation deficit, Fig. 3.25.

F. EXPERIMENTAL SIMULATION

Based upon the results of this study, research into the problem of cloud thickness prediction and shortwave radiation deficit has begun. Case I variables (Table I) were used to initialize a revised version of the model, Figs 3.26 and 3.27. Of major concern is the difference in the predicted evolution of cloud thickness. The uncoupled and coupled models predicted clouds of thicknesses ranging from

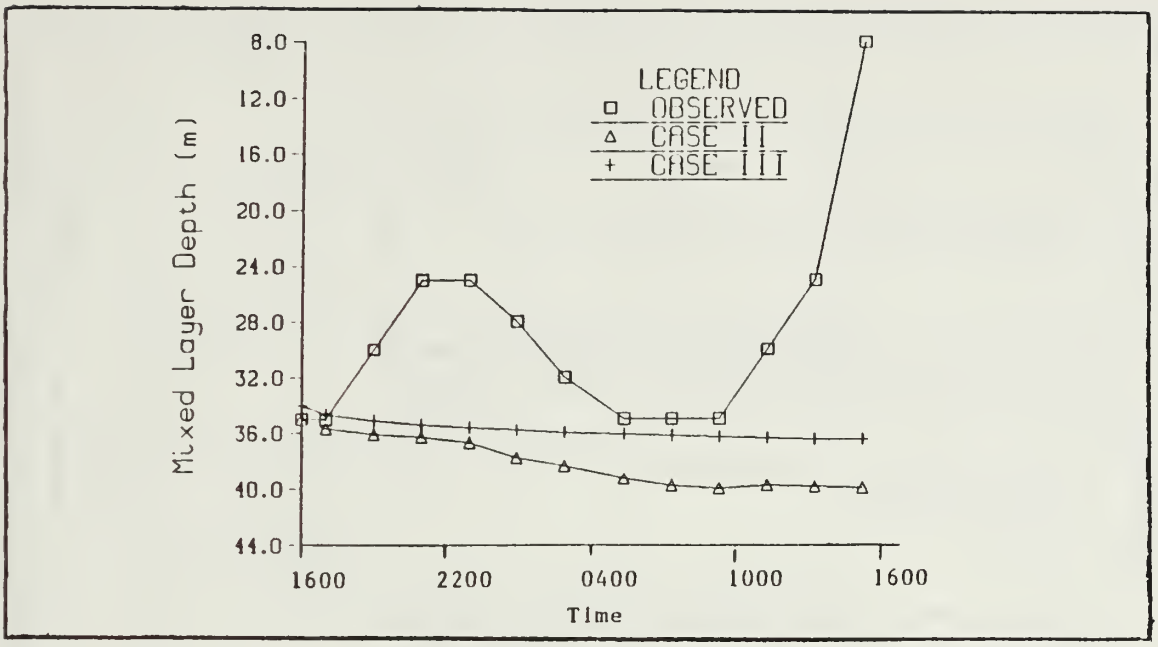

Figure 3.24 Mixed Layer Depth

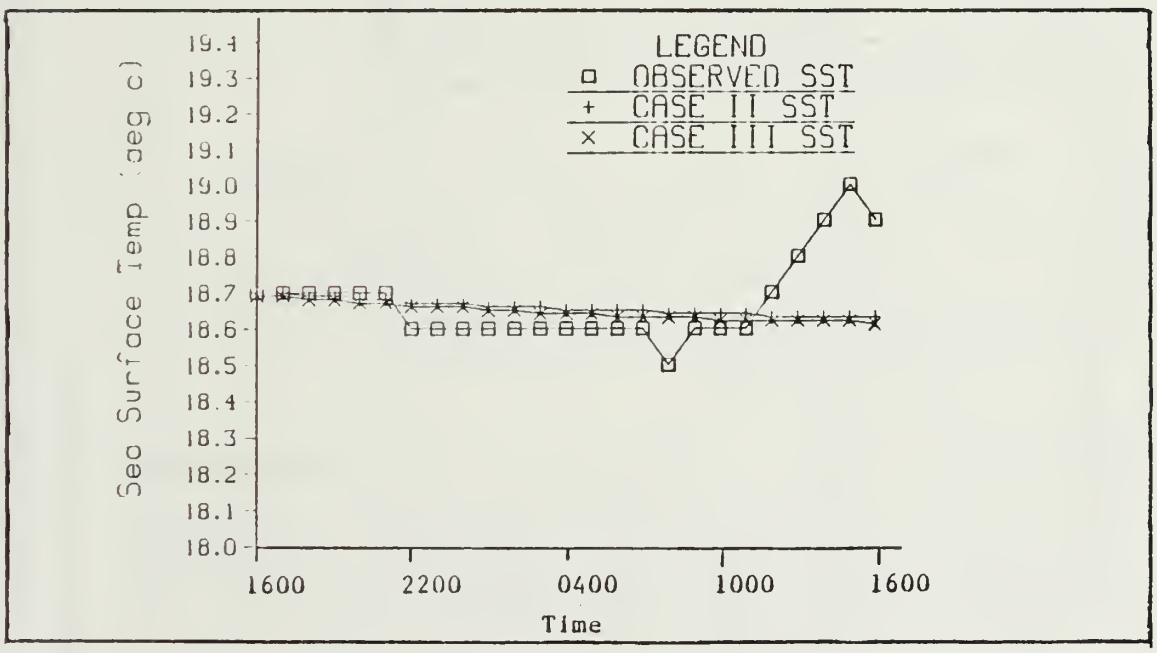

Figure 3.25 Sea Surface Temperature
Coupled Model

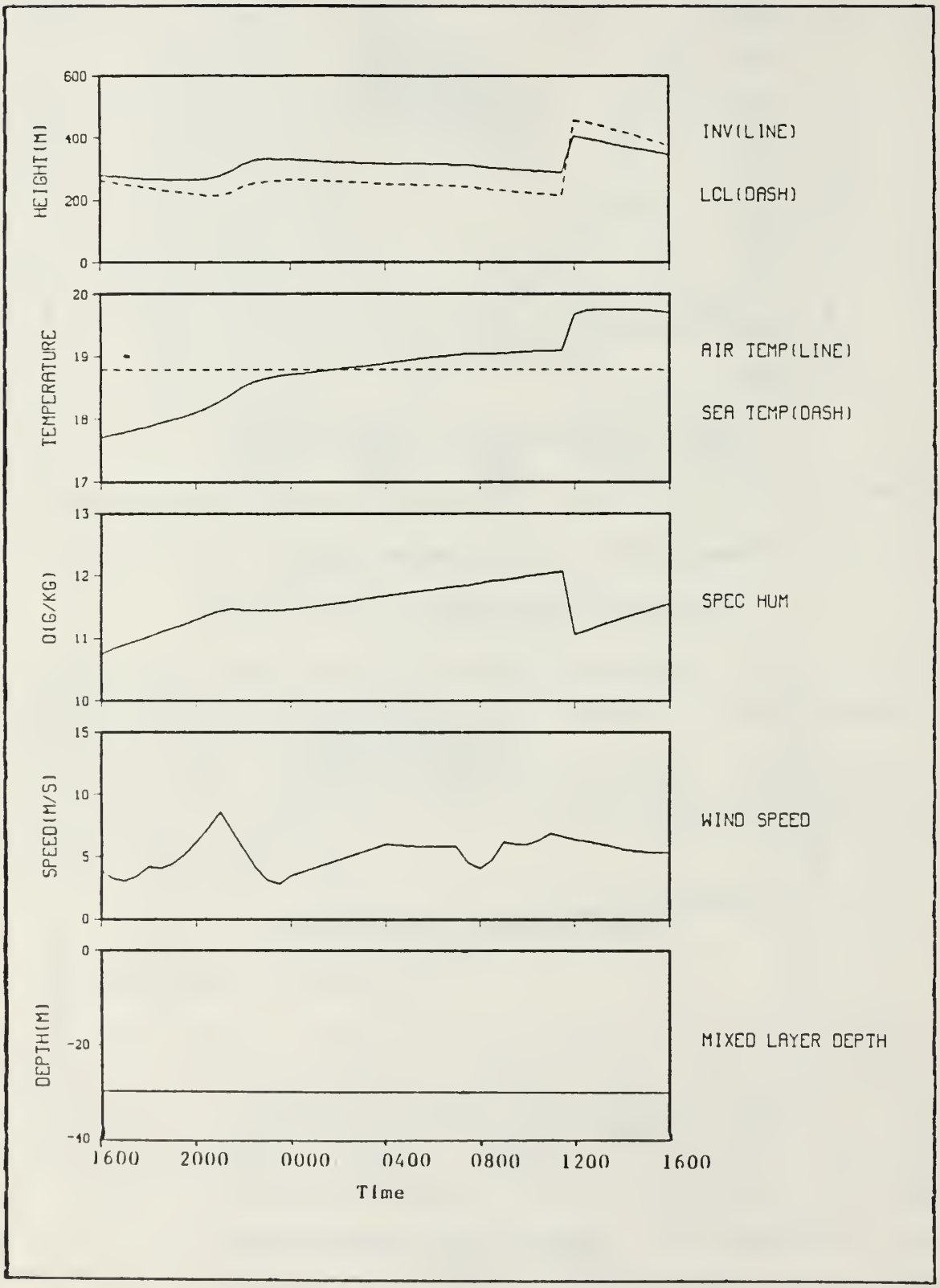

Figure 3.26 Uncoupled Model Revised

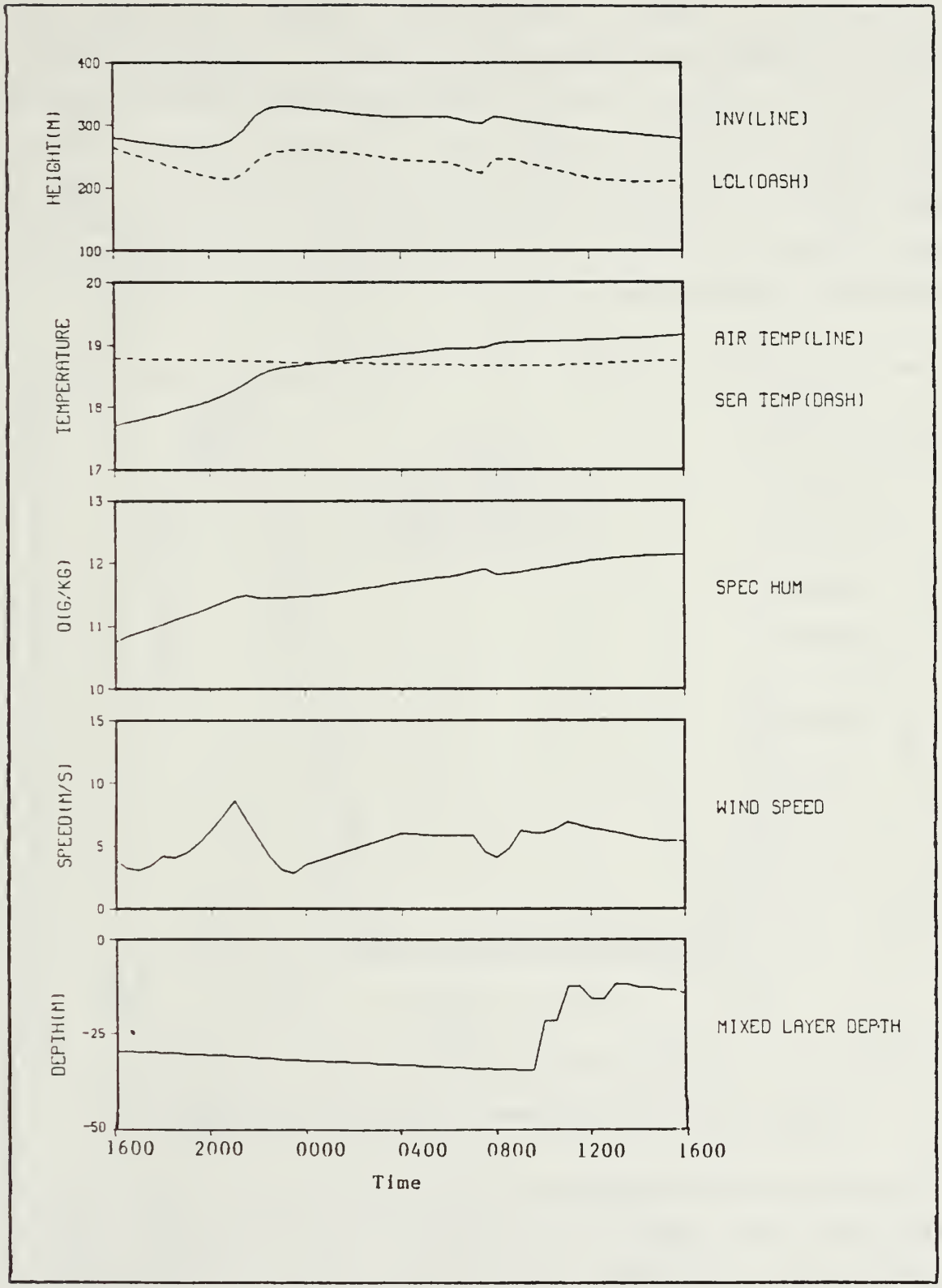

Figure 3.27 Coupled Model Revised

50 to 100 m. Case I clouds were originally predicted to attain a thickness of 635 m (Fig. 3.26). Predicted values of shortwave radiation are in better agreement with observations (as compared with prior cases) although differences do exist, Fig. 3.28. Mixed layer depth was predicted to shallow whereas the earlier cases demonstrated only deepening. This too was a result of the difference in the predicted evolution of shortwave radiation.

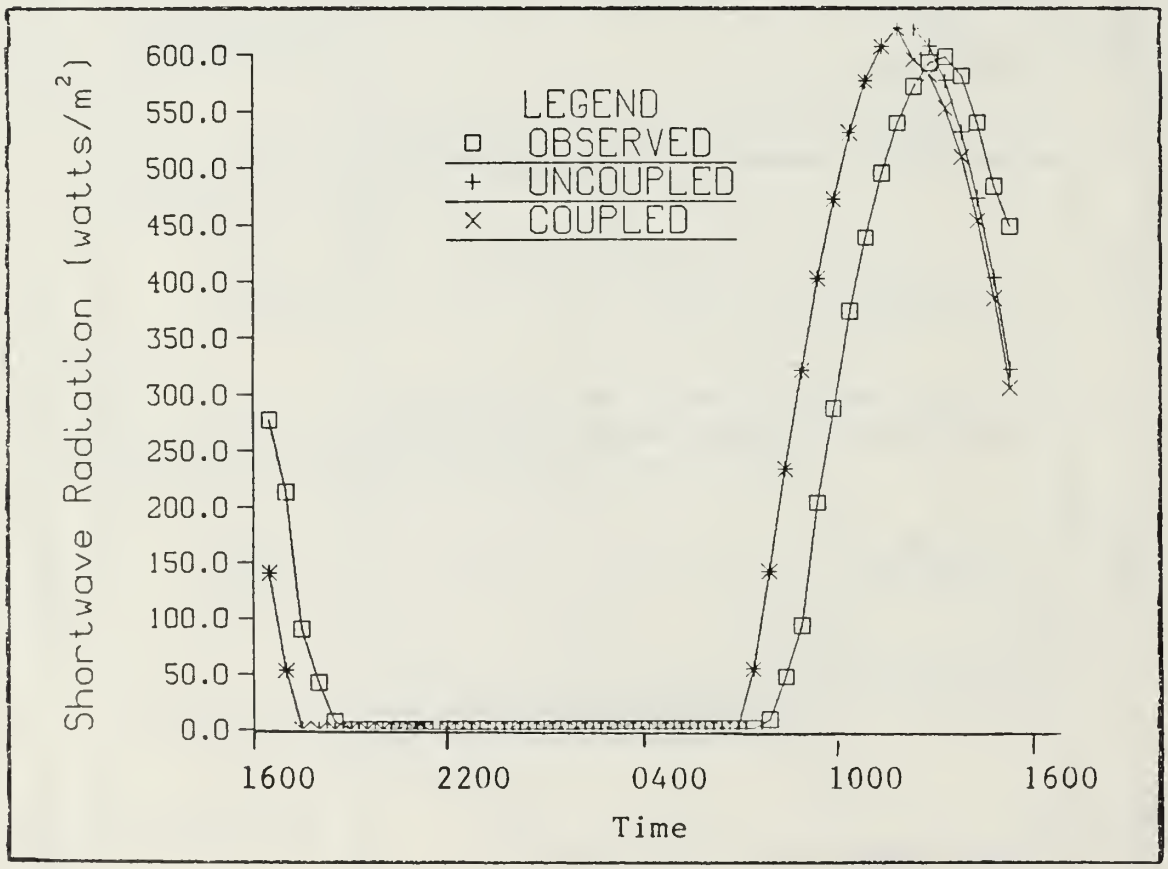

Figure 3.28 Shortwave Radiation Comparison

The evolution of predicted inversion height, LCL, air temperature and specific humidity by the uncoupled model demonstrated an extreme jump 20 hours after initialization (1200 04 Nov). As demonstrated previously, dynamic feedback

continued to occur among the predicted variables. Variations of such magnitudes however, over a period of less than 30 minutes are unrealistic.

IV. CONCLUSIONS/RECOMMENDATIONS

Uncoupled and coupled model predictions overestimate cloud thickness and assume an unrealistic horizon to horizon cover. As a result, short and long wave radiative effects are minimized. The impact of this discrepancy affects all of the model's physics as the fluxes of heat and moisture, variation of sea surface temperature and mixed layer depth are improperly forced. Hence, the values for boundary layer variables such as specific humidity, air temperature, LCL and inversion height differ from observations.

Given this shortcoming, the model demonstrates little variation between the coupled and uncoupled models. The value of oceanic-atmospheric coupling has been documented (O'Lauglin, 1982). The model behaves well for an extended period (48 hours) when reinitialized after 24 hours.

The preliminary results obtained through the use of a modified version of the model indicated that the model will predict commonly observed variations in parameters such as mixed layer depth. Similar predictions can be obtained through the use of different experimental initializing variables. The key question which must now be investigated is why did the original coupled and uncoupled models behave as they did with the MILDEX observations. Due to the tentative nature of these results, definitive conclusions concerning the radiation and cloud modeling as it now exists cannot be drawn. The MILDEX data set is somewhat limited in its applicability due to gaps in the many variables required to initialize the model. The main advantage of the data set was the lack of platform motion during the exercise, thus limiting advective effects which such motion may introduce. The data set should continue to be valuable in future studies with this model.

Cloud physics modeling must continue to be reviewed along with verification and sensitivity analyses. A multi-layer cloud model should be incorporated to examine radiation prediction. Though adequate, the slab approach currently employed is no longer essential as a means of reducing computation time. Additionally, a capability to account for partial cloudiness is absolutely essential. The total cloud cover assumption currently employed has been demonstrated by this study to be the most serious shortcoming of an otherwise fundamentally sound model. A statistical approach in the description of cloud cover percentage is suggested as a possible solution. Further study is essential in this area.

The model should remain in a research phase of development and not be distributed for operational evaluation until the problems outlined herein are rectified. Once the model has been further refined to alleviate these problems, it should then be incorporated into a tactical environmental prediction model. Then the model will be a useful tool for the Oceanography Officer in support of fleet operations.

As for data acquisition, the performance of a navaid radiosonde system should be analyzed. The inability to record pressure and altitude for several launches severly restricted the amount of useful radiosonde data in MILDEX. Additionally, graduate student involvement in data acquisition experiments is essential. Such an individual would be able to acquire a background on the data base and the atmospheric and oceanic situation. An exercise conducted in an area such as Monterey Bay would be useful. Such a limited body of water would further limit the advective effects of the open ocean.

LIST OF REFERENCES

Araya, S.P.S., 1972: The condition for the maintenance of turbulence in stratified flows. Quart. J. Roy. Meteor. Soc., 98, 264-273.

Businger, J.A., 1973: Turbulent transfer in the atmospheric surface layer. Workshop on Micrometeorology, D.A. Haugen, Ed., Amer. Meteor. Soc., 392 pp.

Davidson, K.L., C.W. Fairall, P.J. Boyle, and G.E. Schacher, 1984: Verification of an atmospheric mixed-layer model for a coastal region. J. Climate Appl. Meteor., 617-636.

Fleagle, R.G., and J.A. Businger, 1980: An Introduction to Atmospheric Physics. 2nd ed. Academic Press, 432 pp.

Garwood, R.W. Jr., 1977: An ocean mixed layer model capable of simulating cyclic states. J. Phys. Oceanogr., 7, 455-468.

Geernaert, G.L., P.S. Guest, C.E. Skupniewicz, D.E. Spiel, K.L. Davidson, W.J. Shaw, K.B. Katsaros, and R.J. Lind, 1984: Meteorology report for the 1983 Mixed Layer Dynamics Experiment (MILDEX). Tech. Rep. NPS-63-84-002, Naval Postgraduate School, Monterey, Ca., 128 pp.

Gleason, J.P., 1982: Single station assessments of the synoptic scale forcing on the marine atmospheric boundary layer. M.S. Thesis, Naval Postgraduate School, Monterey, Ca., 55 pp.

Hervey, R.V., 1983: Sensitivity analys of a coupled atmospheric-oceanic boundary layer model. M.S. Thesis, Naval Postgraduate School, Monterey, Ca, 61 pp.

Husby, D.M., and G.R. Seckel, 1978: Large scale air-sea interactions at ocean station V. NOAA Tech. Rep. NMFS SSRF-696, 44 pp.

Joseph, J.H., W.J. Wiscomb, and J.A. Weinman, 1976: The delta-Eddington approximation for radiative flux transfer. J. Atmos. Sci., 33, 2452-2459.

Miller, J.R., 1976: The salinity effects in a mixed layer ocean model. J. Phys. Oceanogr., 6, 29-35.

O'Laughlin, M.C., 1982: Formulation of a prototype atmospheric and oceanic boundary layer model. M.S. Thesis, Naval Postgraduate School, Monterey, Ca., 89 pp.

Slingo, A.S., S. Nicholls, and C.L. Wrench, 1982: A field study of nocturnal stratocumulus: III, High rsolution radiative and microphysical observations. Quart. J. Roy. Meteor. Soc., 108, 145-166.

Stage, S.A., and J.A. Businger, 1981: A model for entrainment into a cloud topped marine boundary layer-part I: model description and application to a cold air outbreak episode. J. Atmos. Sci., 38, 2213-2229.

Tennekes, H. and A.G.M. Dreidonks, 1981: Basic entrainment equations for the atmospheric boundary layer. Bound. Layer Meteor., 20, 515-531.

INITIAL DISTRIBUTION LIST

No.		Copies
1.	Defense Technical Information Center Cameron Station Alexandria ,VA 22314	2
2.	Library, Code 0142 Naval Postgraduate School Monterey, CA 93943	2
3.	Professor C.N.K. Mooers, Code 68Mr Naval Postgraduate School Monterey, CA 93943	1
4.	Professor R.J. Renard, Code 63Rd Naval Postgraduate School Monterey, CA 93943	1
5.	Professor R.W. Garwood, Code 68 Gd Naval Postgraduate School Monterey, CA 93943	3
6.	Professor K.L. Davidson, Code 63Ds Naval Postgraduate School Monterey, CA 93943	3
7.	Professor C.R. Dunlap, Code 68Du Naval Postgraduate School Monterey, CA 93943	1
8.	Director Naval Oceanography Division Naval Observatory 34TH and Massachusetts Ave. NW Washington, D.C. 20390	1
9.	Commander Naval Oceanography Command NSTL Station Bay St. Louis, MS 39522	1
10.	Commanding Officer ATTN: LCDR John Burger Naval Oceanography Office NSTL Station Bay ST. Louis, MS 39522	1
11.	Commanding Officer Fleet Numerical Oceanography Center Monterey, CA 93940	1
12.	Commanding Officer Naval Ocean Research and Development Activity NSTL Station Bay St. Louis, MS 39522	1
13.	Commanding Officer Naval Environmental Prediction Research Facility Monterey, CA 93940	1

14.	Chairman Oceanography Department U.S. Naval Academy Annapolis, MD 21402	1
15.	Chief of Naval Research 800 N. Quincy Street Arlington, VA 22217	1
16.	Office of Naval Research (Code 422) Naval Oceanography Research and Development Activity NSTL Station Bay St. Louis, MS 39522	1
17.	Scientific Liaison Office Office of Naval Research Scripts Institute of Oceanography La Jolla, CA 92037	1
18.	Library Scripps Institute of Oceanography P.O. Box 2367 La Jolla, CA 92307	1
19.	Commander Oceanographic Systems Pacific Box 1390 Pearl Harbor, HI 96860	1
20.	LCDR Joseph W. Swaykos Naval Oceanography Command Detachment Box 57, Naval Air Station Brunswick, ME 04011	2
22.	Commanding Officer Naval Oceanography Command Facility NAS North Island San Diego, CA 92135	1
23.	Dr. T. Spence (Code 422PO) Office of Naval Research 800 North Quincy St. Arlington, VA 22217	1
24.	Dr. Paul Twitchell (Code 331C) Naval Air Systems Command Washington, D.C. 20360	1

213139

Thesis
S9269
c.1

Swaykos
Simulation of the coupled atmospheric and oceanic boundary layer model during MILDEX.